The ER-PM interaction is essential for cytokinesis and recruits the actin cytoskeleton through the SCAR/WAVE complex

Zhijing Xu[1,2], Jingze Zang[1,2], Xintong Zhang[1,2], Qiwei Zheng[1,2], Yifan Li[1,2], Nadine Field[3], Jindriska Fiserova[4], Bing Hua[5], Xiaolu Qu[1,2], Verena Kriechbaumer[3], Michael J. Deeks[6], Patrick J. Hussey[4], Pengwei Wang[1,2]*

1. National Key Laboratory for Germplasm Innovation & Utilization of Horticultural Crops, College of Horticulture and Forestry Sciences, Huazhong Agricultural University, Wuhan 430070, China; 2. Hubei Hongshan Laboratory, Wuhan, 430070, China; 3. School of Biological and Medical Sciences, Oxford Brookes University, Oxford OX3 0BP, UK; 4. Department of Biosciences, Durham University, South Road, Durham, DH1 3LE, UK; 5. College of Horticulture and Landscape Architecture, Yangzhou University, Yangzhou, 225009, China; 6. Biosciences, University of Exeter, Stocker Road, Exeter EX4 4QD, UK.

For correspondence: wangpengwei@mail.hzau.edu.cn

Author Contributions:

Z.X. performed most of the experiments and wrote the manuscript with P.W.; P.W. conceived and supervised the project; X.Z., Y.L., and J.Z. helped generate transgenic lines and analyze data; N.F. and V.K. performed the SBEM study; B.H. helped with the pull-down assay; Q.Z performed the TEM study; J.F. and M.J.D performed the original Y2H screen and i*n vitro* pulldowns under the supervision of P.J.H. X.Q., M.J.D., and P.J.H. provided critical advice throughout the study and edited the manuscript

Competing Interest Statement: The authors declare no competing interests.

Data share plans: All study data are included in the article and/or supporting information.

Classification: Biological Sciences; Plant Biology.

This PDF file includes:

Main Text
Figures 1 to 7
Figures S1 to S6
Tables S1 to S3

Abstract

Plant cytokinesis requires coordination between the actin cytoskeleton, microtubules and membranes to guide division plane formation and cell plate expansion; how these regulatory factors are coordinated remains unknown. The actin cytoskeleton assembly is controlled by several actin nucleation factors, such as the SCAR/WAVE complex, which regulates actin nucleation and branching through the activation of the ARP2/3 complex. The activity of these actin regulatory proteins is likely influenced by interactions with specific membranes; however, the molecular basis and the biological relevance of SCAR-membrane interactions are also unclear. In this study, we demonstrate that the ER-PM tethering protein VAP27-1 directly interacts with SCAR2 at the ER membrane, and that they co-localise to guide cell plate orientation during cell division. In the root meristem, both VAP27-1 and SCAR2 exhibit polarised localisation at the cell plates, where the interaction between ER and PM is abundant. VAP27-1 recruits SCAR2 to the cell division plane, where there is a high concentration of actin filaments. In the *vap27-1346* mutant, the densities of cortical ER, SCAR2 and consequently actin filaments are significantly reduced at the cell division plane, affecting cell plate orientation, cell division and root development. A similar phenomenon is also observed in the *scar1234* mutant, suggesting that VAP27 and SCAR proteins regulate cell division through a similar pathway. In conclusion, our data reveal a plant-specific function of VAP27-regulated ER-PM interaction and advance our understanding of plant ER-PM contact site and its role in cell division.

Keywords: ER-PM contact sites, Actin cytoskeleton, Endoplasmic Reticulum, SCAR/WAVE complex, Cytokinesis, Cell plate

Significance Statement

Plant cytokinesis requires the contribution of the cytoskeleton and membrane systems, but how actin interacts with these membrane structures is poorly understood. Here, we demonstrate that the VAP27-regulated ER-PM interaction is critical for recruiting the ER network to the cell division plane together with SCAR, which is part of a complex known to activate actin polymerisation. These findings reveal a plant-specific function of the ER-PM contact sites and advance our understanding of cytoskeleton-membrane interactions and their role in cell division.

Main Text

Introduction

The actin cytoskeleton is a highly dynamic structure that regulates many biological activities in plants, such as organelle movement, cell morphogenesis and polarised cell growth. It assembles and disassembles rapidly in response to different environmental and developmental cues, and this rapid remodelling is regulated by specific actin-binding proteins. The ARP2/3 complex is one of the best-known regulators that control actin nucleation, assembly, and branching (1), maintaining cytoskeletal homeostasis and normal plant development (2). The activity of the ARP2/3 complex is controlled by various nucleation-promoting factors, such as the SCAR/WAVE complex that is composed of five different subunits (SCAR, NAP1, PIR121, ABI1 and BRICK1/HSPC300), with the SCAR subunit playing central roles. There are four SCAR homologues identified in the *Arabidopsis* genome; it contains a C-terminal VCA domain that binds to the ARP2/3 complex and an N-terminal SH domain that interacts with other subunits required for actin nucleation (3-5). The sequence similarity of plant SCAR is very low compared to its animal homologues, suggesting it might be involved in unique activities in plants. For example, SCAR2 exhibits polarised localisation in epidermal cells and root hairs, regulating root hair development and asymmetric cell division (6-8). Several members of the ARP2/3 and SCAR/WAVE complexes have been reported to interact with membrane structures to participate in different activities

(9, 10), such as mediating light signal transduction and autophagy (11-13). In plants, these proteins were likely enriched in the ER network, but whether such ER association is essential for the activity of SCAR/WAVE is not known (9).

The endoplasmic reticulum (ER) is a complex membrane network whose dynamics are mainly driven by the actin cytoskeleton in plants (14-19). Cortical ER is also closely associated with the plasma membrane (PM) through several ER-PM tethering proteins at the membrane contact sites (MCS) (20, 21). VAP27 is the plant homologue of the yeast Scs2 protein, which localises at ER-PM contact sites (EPCS) and interacts with actin filaments and microtubules, suggesting that a close interaction among ER, PM, and the cytoskeleton exists in plants (18, 22). Further studies revealed that plant-specific cytoskeletal binding proteins are associated with the EPCS, such as the NET (NETWORKED) and IQD (IQ67 DOMAIN proteins) family, which regulate the organisation of actin and microtubules, respectively (23-25). It is well known in all eukaryotic cells that the cytoskeleton contributes to membrane dynamics and organisation. However, recent studies in plants suggested that membrane structure can also influence cytoskeletal function. When the ER morphology is altered by over-expressing some ER shaping proteins, the distribution and density of actin filaments also changes accordingly (14), indicating some cytoskeletal regulators may associate with the ER surface through an unknown mechanism.

Cytokinesis in plants requires the formation of the cell plate at the division plane, which contains highly ordered microtubule bundles and actin filaments (26-28). In most previous studies, the importance of microtubules in cell division plane establishment has been well reported (29-31), and the roles of actin have only started to be elucidated. It has been shown that myosin motor proteins play a crucial role in cell division, particularly in cell division plane orientation. In the myosin XI-K triple knockout mutant, an increase in the number of oblique cell walls was observed (32). In *Physcomitrium patens,* myosin VIII and XI play a role in guiding cell plate expansion, and their function is dependent on actin nucleating protein *Pp*Formin 2 and the actin cytoskeleton (33, 34).

Some transmission electron microscopy (TEM) and laser confocal microscopy (LCM) studies also revealed that the cisternae ER branch forms narrow ER tubes across the cell plate (35-38). The ER membrane is accumulated at the edge of the cell plate, facilitating the expansion and fusion with the parent cell (39). In *Physcomitrium patens*, interrupting ER function by knocking out some ER localised protein (e.g. SABRE) leads to abnormal cell plate development (40), suggesting the ER is an essential regulator of plant cytokinesis. Still, its mechanisms of action are largely unknown. In fission yeast, the ER-PM contact sites and Scs2 protein restrict the assembly of the actin contractile ring to determine the division sites and define actomyosin kinetics (41). In plants, the disruption of actin also delays cell plate expansion and inhibits the ER accumulation in the cell plate during cytokinesis (42). Therefore, there must be a precisely coordinated mechanism that regulates microtubules, actin and ER networks during cell plate formation. On the other hand, as the cell plate and cell division plane are enriched in cytoskeletal components, PM, and the ER network, it might be considered a specialised region that consists of intensive ER-PM interactions.

In this study, we demonstrate a direct interaction between the ER-PM tethering protein, VAP27 and SCAR, a member of the SCAR/WAVE complex, and that they exhibit a polarised localisation at the newly formed cell plates. The recruitment of SCAR, actin filaments and ER membrane to the cell plate is inhibited in the absence of VAP27. In *vap27-1346* and *scar1234* mutants root development, meristem cell number and cell plate orientation are significantly affected, suggesting that VAP27 underpins SCAR-regulated actin assembly during cell division and cell plate expansion. Taken together, our findings provide solid evidence that the ER and ER-PM interactions are essential for cytokinesis and are reliant on the interaction between VAP27 and SCAR proteins.

Results

SCAR2 was identified to interact with VAP27 from a yeast two-hybrid screen

The SCAR/WAVE and ARP2/3 complexes are essential for actin assembly and dynamics, and this regulatory module is conserved in most eukaryotic cells. In animals, these actin nucleators are required for cell movement and embryogenesis, which is essential for life (43). However, mutating proteins of the SCAR/WAVE complex in plants does not cause lethality, allowing the underlying effects of these mutations to be studied (10, 44). To further understand the regulatory mechanism of the SCAR/WAVE complex in plants, we performed a yeast two-hybrid screen using SCAR2 (a key component of the complex). We identified a possible interaction with VAP27 (Table S1, Fig. S1), a family of conserved integral ER membrane proteins that are also known as VAMP-associated proteins (VAPs) and Scs2 in animals and yeast, respectively (22). Ten VAP homologs have been identified in *Arabidopsis*, and most proteins of this family are localised to various ER-membrane contact sites (40), with the ER-PM contact sites being the most well-studied. First, we constructed the pVAP27-1:VAP27-1-mCherry (hereafter VAP27-mCh) and p35S: GFP-SCAR2 (hereafter GFP-SCAR2) vectors and transiently transformed them into *N. benthamiana* leaf epidermal cells. When both proteins are co-expressed, VAP27-mCh recruits GFP-SCAR2 onto the ER membrane; in contrast, the SCAR2 is solely cytoplasmic when it expressed alone (Fig. 1A). In agreement with this observation, the bimolecular fluorescence complementation (BiFC) assay also suggested that most of the nYFP-SCAR2 and cYFP-VAP27-1 interacting signals were ER-associated (Fig. 1B). This interaction was further confirmed *in vitro* using a GST pull-down assay, the full-length MBP-VAP27-1 protein stays associated with a GST-SCAR2 truncational mutant (a.a. 1-432, Fig. 1C). In *Arabidopsis*, the VAP27 and SCAR proteins have multiple homologues (3, 4, 45), so one-on-one yeast two-hybrid tests were performed between combinations of different VAP27 and SCAR isoforms. The results indicate that SCAR1, 2 and 3 have the capacity to interact with multiple VAP27 proteins (Fig. 1D), suggesting the interaction is likely conserved among different members of the two families. Here, we concentrated on the interaction between VAP27-1 and SCAR2 for most cell biology and microscopical studies to avoid repetition.

Next, we obtained transgenic *Arabidopsis* lines stably expressing VAP27-1-GFP (hereafter VAP27-GFP) and SCAR2-mCherry (hereafter SCAR2-mCh) driven by its native promoters (6, 45). Both proteins are globally expressed with the strongest signals at the root tips. Subsequent observation revealed that VAP27-1 is localised at the cell peripheral and the ER membrane, while SCAR2 is mainly at the PM in root cells (Fig. 1E, F). Interestingly, both proteins exhibit polarised localisation and co-localised at the transverse cell interface, as indicated in the high magnification images (Fig .1G, H). Fluorescence signal intensity analysis further supports that VAP27-1 and SCAR2 are highly enriched in the apical/basal plasma membrane, with a higher axial-to-lateral signal ratio on the PM. In contrast, the signal ratio of FM4-64 labelled PM is close to 1.0, indicating a non-polarised localisation (Fig. 1I). In addition, there was an enrichment of SCAR2 at the cell corners, which may be related to stronger local actin polymerising activity and root cell elongation (Figure S7); a similar behaviour was seen for other SCAR/WAVE subunits (e.g. BRK1 and NAP1; 12, 46).

SCAR2 and VAP27 regulate primary root growth and affect the cytokinetic activity of root meristems

To gain further insight into the biological relevance of the SCAR and VAP27 interaction, we performed phenotypical analysis using the *scar1234* quadruple mutant (T-DNA insertional mutant of SCAR1, 2, 3 and 4) and the *vap27-1346* quadruple mutant (CRISPR knock-out of four VAP27 genes, VAP27-1, -3, -4 and -6). These lines were obtained from previous publications and validated as functional knock-out mutants (46, 47). We mainly focused on root tissue where SCAR2 and VAP27 are co-expressed and found the primary root of both *scar1234* and *vap27-1346* mutant seedlings are significantly shorter than the wild type (Fig. 2A, B). Such a defect was likely caused by a reduced number of meristem cells and a shorter meristem region (Fig. 2C-J). To further determine the function of SCAR and VAP27 in the root meristem, 3-day-old seedlings were stained with DAPI and 5-ethynyl-20-deoxyuridine (EdU), which selectively labels the nucleus of newly divided cells. Image quantification of the EdU/DAPI ratio showed that the number of newly divided cells was significantly

reduced in the *scar1234* and *vap27-1346* mutants, consistent with the observation of reduced meristem size (Fig. 2K, L). Both *scar1234* and *vap27-1346* also show similar defects in pavement cell morphogenesis (Fig. S2A-E), a process regulated by the actin cytoskeleton.

In addition, the seedlings of *vap27-1346* mutants also show a twisted root phenotype (Fig. 2B). Therefore, the root epidermal cells of *vap27-1346* were studied in-depth using propidium iodide (PI) staining (Fig. 2M), and the results suggested that the cell organisation is different. In the wild-type, the transverse cell wall is almost perpendicular to the growth direction; however, their orientations are highly variable in the *vap27-1346* mutant (Fig. 2N), indicating the direction of cell division is likely affected. Given these findings and the conserved function of SCAR in actin nucleation and branching, we hypothesise that the root phenotype observed in *vap27-1346* is likely related to defects in the assembly of actin filaments. To test this hypothesis, wild-type *Arabidopsis* seedlings were germinated on 1/2 MS medium containing a low concentration of an actin polymerisation inhibitor, latrunculin B (Lat B). Similarly, shorter primary roots, reduced meristem size and disorganised cell division patterns were also observed (Fig. S3A-F), indicating the root phenotype in the *vap27-1346* mutant is likely to be actin cytoskeleton related. Actin density at the division plane is significantly reduced after the mild Lat B treatment (200 nM), while the ER density (as indicated by VAP27-mCherry) hardly changes (Fig. S3G-I).

Taken together, these results indicate that the interaction between the actin nucleation factor SCAR and the EPCS protein VAP27 is likely essential for root growth and meristem maintenance. Knocking out the VAP27 proteins may inhibit actin assembly (mimicking the phenotype of Lat B treatment), ultimately affecting cell division and root meristem defect. As the VAP27 and SCAR mutants showed similar phenotypes, we speculated that both proteins are likely to act in a shared pathway (please refer to the results related to figures 5 and 6 later).

The cortical ER network and ER-PM interaction are involved in cell plate formation

Previous studies found that the ER membrane is highly enriched at the division plane and the developing cell plates (42), but the exact function of the ER in plant cytokinesis is unknown. In plants, the ER-PM tethering protein VAP27 is also associated with the cytoskeleton network at the ER-PM contact sites (15, 16, 20, 21, 24, 25). Given the involvement of VAP27 in *Arabidopsis* root growth and meristematic cell patterning (Fig. 1F, G), we speculated that the ER network and ER-PM interaction could be involved in cell division and cell plate formation. To address this question, we generated stable *Arabidopsis* lines expressing an artificial EPCS marker (MAPPER-GFP) under the control of a ubiquitin promoter (48). In root meristems, both MAPPER-GFP and VAP27-GFP showed polarised localisation at the transverse cell junction (Fig. S5C-F), and their signal strongly overlapped with FM4-64. Similar behaviour is not very prominent in GFP-HDEL (a general ER marker; Fig. S5A, B) expressing lines (49), suggesting the ER signal enrichment at the cell junction likely requires ER-PM tethering.

To better understand the differential behaviour between the ER and EPCS markers, we studied the late cytokinesis process using different transgenic lines. FM4-64 is employed as a cell plate marker as it labels newly synthesised membrane at the division plane (Fig. 3). In contrast to the localisation of GFP-HDEL, the signals of EPCS markers (MAPPER-GFP, VAP27-GFP) are more enriched at the cell plate (Fig. 3A-C), suggesting ER-PM interactions are likely very abundant at the cell plate region. The ER labelling at the cell plate gradually increases during the telophase, reaching its highest point as it matures (Fig. 3A, C). Serial-block face SEM (SBEM) studies further confirmed this observation at the ultrastructural level, with massive accumulations of ER membrane associated with both sides of the cell plate (Fig. 3D and Video S1). In summary, these results indicate that the ER membrane is closely associated with the cell plate, and this specific membrane interaction probably involves ER-PM tethering

factors (e.g. VAP27, Fig. 3C). Therefore, we investigated the function of the VAP27-SCAR2 interaction and ER-actin association during cytokinesis.

VAP27 recruits SCAR to regulate cell plate expansion and actin assembly.

According to the subcellular localisation and phenotypic study of VAP27-1 and SCAR2, we speculated that both proteins might contribute to root meristem maintenance through regulating cytokinesis. Confocal microscopy observation revealed that VAP27 was initially enriched at the cell division plane since the late anaphase (Fig. S6). In contrast, the signal of SCAR2 was more evident from the telophase (Fig. 4A). Further quantification confirmed that the fluorescence intensity of SCAR2 showed a gradual increase at the late telophase. In contrast, the VAP27 signal increases before that (Fig. 4A, B). ~~At the late telophase, both SCAR2 and VAP27 were particularly enriched at the edge of cell plates (Fig. 4A, arrows), favouring a hypothesis that both proteins regulate cell plate expansion and subsequent fusion with the parent cell~~. Given the previously demonstrated interaction between VAP27-1 and SCAR2, it is likely that VAP27 accumulates at the division plane first and then recruits SCAR2 sequentially. We tested this hypothesis by studying SCAR2-mCh in different genetic backgrounds. In the *vap27-1346* mutant, the polarised distribution of SCAR2 is affected significantly (Fig. 4C). The fluorescence intensity of SCAR2-mCh at axial and lateral PM was quantified. The result suggested that the SCAR2 signal does not accumulate on the transverse cell interface (Fig. 4D), likely due to the abolished interaction with VAP27, so it cannot be efficiently recruited to the new division plane. Furthermore, the ER fluorescence intensity is significantly reduced in the *vap27-1346* mutant (Fig. 4E); this observation is confirmed by the signal ratio of GFP-HDEL at the division plane and cytoplasm (Fig. 4F). Meanwhile, the TEM images showed a reduction in the density of ER surrounding the cell plate (Fig. 4G).

The actin cytoskeleton is important for cell division and cell plate directional expansion; it is enriched alongside the preprophase band (PPB) and defines the cell division plane with microtubules (50-52). In the *Arabidopsis* root, F-actin accumulated

at the apical-basal plasma membrane, which might determine cell polarity during cell division (53). As SCAR2 promotes actin elongation and branching, transgenic *Arabidopsis* lines expressing SCAR2-mCh or VAP27-1-mCh were crossed with an actin marker line (GFP-Lifeact) to study the behaviour of actin and ER during cytokinesis. As the cell plate expands at telophase, there is a significant accumulation of actin bundles at the division plane, together with VAP27 and SCAR2 (Fig. 5A, B), whereas the signal of VAP27 is enriched at the leading edges in particular (Fig. 5B, arrow). In both *vap27-1346* and *scar1234* mutant, the fluorescence intensity of actin was significantly reduced at the cell division plane and transverse cell interface of root epidermal cells (Fig. 5C-F). In addition, we measured the maximum length of cell plates at different time points and calculated the cell plate expansion rate as micrometre per minute. The results showed that the growth rate of cell plates in the *vap27-1346* is significantly slower than Col-0 (Fig. 5G, H and Video S2-S3).

Taken together, these results suggest that VAP27 modulates SCAR and actin recruitment, forming a VAP27-SCAR-actin macromolecular complex that facilitates ER-PM interaction and actin nucleation at the division plane, ultimately affecting the speed and direction of cell plate expansion and root development.

The function of SCAR2 requires VAP27 interaction.

According to the protein interaction results and mutant phenotype studies, it is likely that VAP27 and SCAR2 regulate cell division and root development in a coordinated way; therefore, we then addressed whether the interaction of VAP27 is essential for SCAR2 function. First, we generated a number of SCAR2 truncations to determine the motif required for the interaction. Through a yeast two-hybrid assay, we found the N-terminal sequence of SCAR2 (a.a. 1-432) is sufficient for VAP27 interaction, and subsequent truncation of $SCAR2^{1-432}$ further narrowed this interacting motif to a.a. 340-432 (Fig. 6A, B), which contains three linear interactive peptides (LIPs) as predicted by MobiDB (54). It has been shown that the LIP peptides are likely involved in protein interactions (55). In yeast and animals, the FFAT motif (consecutive phenylalanines in

an acidic tract) are recognised by VAP through its major sperm domain (MSD)(55, 56). Using the VAP interactome prediction program (Murphy and Levine, 2016), we have found a FFAT-like motif (LTSEADNYVDAPAT) within the LIP1 peptide (Fig. 6C). Therefore, we suspected that the LIP1 motif (a.a. 357-388) could be essential for the VAP27 interaction in plants. Indeed, yeast two-hybrid and BiFC assays confirmed that deletion of LIP1 (SCAR2$^{\Delta LIP1}$) prevents VAP27-1 interaction (Fig. 5D, E). Meanwhile, the interactions between LIP1 and VAP27-1 have been further validated by AlphaFold3 protein docking prediction (REF, Fig. S7A-B) and *in vitro* pull-down assays (Fig. S7C).

We transformed the pSCAR2:SCAR2-HA and pSCAR2:SCAR2$^{\Delta LIP1}$-HA construct into the *scar1234* quadruple mutant to test whether the LIP1 domain is required for SCAR2 function during cell division. Full-length SCAR2 could complement the meristem and root growth phenotype of the *scar1234* mutant. However, gene complementation using SCAR2$^{\Delta LIP1}$ cannot do the same (Fig. 6F-J), suggesting that the activity of SCAR2 is dependent on the VAP27 interaction, which recruits it to the ER membrane (Fig. 1A). A similar experiment was also performed with VAP27-1. Previous studies indicated that a lysine residue (a.a. 58) and two threonine residues (a.a. 59-60) are indispensable for VAP27-1 to interact with other proteins (22). Therefore, we substituted the lysine for asparagine (VAP27-1^{N}) and the threonine for alanine (VAP27-1^{A}). The mutated VAP27-1 was tested for interaction with SCAR2 via Y2H and BiFC assays, and the results demonstrated that the mutant VAP27-1 could not interact with SCAR2 (Fig. 6K-M). Not surprisingly, both VAP27-1^{N} and VAP27-1^{A} mutant (driven by its native promoter) cannot complement the root phenotype of the *vap27-1346* quadruple mutant, consistent with the conclusion that VAP27-SCAR interaction is important for their function and root development (Fig. 6N-R).

Discussion

Collectively, the ER-PM tethering protein VAP27 recruits ER and SCAR to the cell plate to produce a plant-specific configuration of cytoskeleton ER-PM interaction. Using multiple approaches, we showed that the SCAR of the SCAR/WAVE complex

interacts with VAP27. This macromolecular complex supports cell plate orientation and regulates meristem cell maintenance and root development. In the absence of VAP27, we observed that the contact between the ER membrane and the cell plate is reduced, consequently affecting SCAR recruitment and actin filament formation (Fig. 6).

The position and direction of cell plate formation determine the dimensions of cell proliferation and organ morphology. Previously, numerous studies reported that microtubules are necessary for the synthesis of cell plates (26, 51, 57). Nevertheless, the expansion of the phragmoplast and cell plate are also influenced by actin polymerisation inhibitors (42). At the PPB formation stage, actin polymerisation and rearrangement generate forces on the PPB and define the position of the cell division plane (42-44), ultimately influencing the formation of new cells (31, 51, 52, 58, 59). Moreover, myosins are localised to the edge of the phragmoplast and the cell division site (30-32), where they play a role in ensuring the correct orientation of the cell plate and the accurate recognition of the fusion site on the parent cell (32, 33, 52). This reflects the involvement of actin in determining the direction of cell proliferation, which is crucial for plant growth and morphogenesis. VAP27 is a protein that localises at the ER membrane and ER-membrane contact sites; it also accumulates at the cell division plane where the cell plate is formed (Fig. 1E). Actin likely assembles into short bundles at the phragmoplast, forming the scaffold with microtubules and other proteins to direct vesicle trafficking and cell plate expansion (30). In this study, we show the interaction between VAP27 and SCAR at ~~the edge of~~ the cell plate (Fig. 4A). Further analysis using various mutant and transgenic lines suggest that VAP27 is required for the polarised localisation of SCAR2. In the vap27-1/3/4/6 mutant, the SCAR2 localisation and actin cytoskeleton accumulation at the division plane and transverse cell-cell interface are affected, suggesting VAP27 is able to recruit SCAR to regulate actin density. This process is likely involved in cell plate expansion and directional growth.

In addition to the function of SCAR recruitment and actin nucleation, the VAP27-regulated ER-PM interaction is likely to be involved in many biological activities during cell division. It has been reported that many ER tubules traverse the cell plate

during its formation, eventually forming plasmodesmata (35-38), which provide cytoplasmic and membrane continuity between adjacent cells, facilitating direct communication and transport of molecules between cells. VAP27 has been reported to partially co-localise with plasmodesmata (20, 24), and here we show the accumulation of VAP27 on the cell plate (Fig. 3D), indicating a possible function of VAP27 in plasmodesmata biogenesis. In addition, VAP27 bridges the ER with endocytic membranes and contributes to endocytic trafficking events, which are essential for cell plate maturation and fusion with the parent cell (50).

In summary, the complex assembled by VAP27 recruits SCAR and facilitates ER-PM-actin interaction at the cell plate, which enables the guidance of cell plate expansion and orientation ~~the fusion of cell plates with the parent cell walls at the cell division site~~. In the future, it will be intriguing to study how the functions of the ER, actin and microtubules are coordinated during cytokinesis. The establishment of ER-PM connections could be essential, as the ER-PM contact sites are the place where actin and microtubules converge.

Materials and Methods

Transgenic *Arabidopsis* lines

Transgenic *Arabidopsis* lines pVAP27-1:VAP27-1-GFP (45) and pSCAR2:SCAR2-mCherry have been described previously (6). To generate the ER marker GFP-HDEL (49), EPCS maker MAPPER-GFP (48), and pVAP27-1:VAP27-1-mCherry *Arabidopsis* lines, Col-0 was dipped with these vectors via *Agrobacterium*-mediated transformation. *Arabidopsis* lines co-expressing VAP27-1-GFP + SCAR2-mCherry, GFP-Lifeact + SCAR2-mCherry and GFP-Lifeact + VAP27-1-mCherry were generated by crossing using transgenic plants stably expressing the single construct. The GFP-Lifeact/*vap27-1346* and SCAR2-mCherry/*vap27-1346* were generated by crossing stable transgenic GFP-Lifeact and SCAR2-mCherry plants with the *vap27-1346* mutant.

The *vap27-1346 C64/C44* and *scar1234* mutants were described previously (46, 47). The complementation constructs generated in this study are described below, which were transformed into strain *Agrobacterium tumefaciens* GV3101 and transformed into *Arabidopsis* by floral dip. The complete list of all the plasmids and transgenic *Arabidopsis* lines used in this study can be found in Supplemental Tables 2 and 3.

Molecular cloning

In this study, PCR amplification was performed using Phanta Max Super-Fidelity DNA Polymerase (Vazyme, P505), and the gateway reaction was performed using BP Clonase™ II (Invitrogen) and LR Clonase™ II (Invitrogen). The restriction endonuclease was purchased from NEB, and Cloning was performed using Clone Express II One Step Cloning Kit (Vazyme, C112-01/02). The p35S: GFP-SCAR2 construct used for transient expression was described in a previous paper (5). For the expression of VAP27-1 under its native promoter, pVAP27-1:VAP27-1-mCherry construct was generated. The promoter region (about 2 kb upstream of the start codon) and the genomic sequence of VAP27-1 were amplified by PCR from *Arabidopsis* seedling genomic DNA, and it was then cloned into pMDC107-mCherry plasmid by gateway LR reaction.

For gene complementation assays, the full-length or mutated sequence of VAP27-1 and SCAR2 were fused with the HA-tag by PCR and cloned into pROE-O4 and modified pMDC43 vectors by homologous recombination. The native promoters of VAP27-1 and SCAR2 genes were used to drive their expression, generating pVAP27-1:VAP27-1-HA, pVAP27-1:VAP27-1^{N}-HA, pVAP27-1:VAP27-1^{A}-HA, pSCAR2:SCAR2-HA and pSCAR2:SCAR2$^{\Delta IP1}$-HA. These constructs were transformed into the *vap27-1346* and *scar1234* mutants, respectively.

For the BiFC assay, the CDSs (or the mutated sequence) of VAP27-1 and SCAR2 were cloned into pMDC43-cYFP or pMDC43-nYFP plasmid by gateway reaction. The original template of the VAP27-1 mutants was reported previously (24). The

SCAR2$^{\Delta LIP1}$, SCAR2$^{\Delta LIP2}$ and SCAR2$^{\Delta LIP3}$ deletional mutants were generated by homologous recombination using primers spanning the sequence of LIP1, 2 or 3. For the Y2H assay, the CDSs of the SCAR and VAP27 genes were amplified from a cDNA library generated from *Arabidopsis* seedling. The full-length and truncated fragments of SCAR and VAP27 were cloned into the pGADT7 and pGBKT7 vectors, respectively. For the protein purification assay, the CDSs of truncated SCAR2 (a.a. 1-432) and VAP27-1 were cloned into glutathione S-transferase (GST) in pGEX-4T1 and maltose-binding protein (MBP) in pMAL-c5X vector by DNA recombination. The lists of constructs and primers used in this study were summarised in Supplemental Tables 2 and 3.

Confocal microscopy and Image analysis

N. benthamiana leaf infiltration was used for transient expression and BiFC assays. To do this, the plasmids were transformed in *A. tumefaciens* GV3101 and pressure-infiltrated into the abaxial epidermis of *N. benthamiana* leaves. After 3 days of cultivation, the transformed leaves were imaged by confocal microscopy (Leica TCS SP8) with 40 × water and 63 × oil immersion objectives. For the study of *Arabidopsis* seedlings and the cytokinesis process, seedlings were grown on 1/2 MS solid medium for two days and stained with DAPI or FM4-64 if necessary. Samples were mounted on microscope slides with 0.1% low melting point agarose and imaged using a Leica TCS SP8 confocal microscope. For the time-series acquisition, samples were mounted between the slide and the coverslip with a thin layer of 1/2 MS medium. The excitation wavelengths for DAPI, GFP, YFP and mCherry/PI/FM4-64 were 405 nm, 488 nm, 514 nm and 552 nm, respectively. Emission was detected between 410 and 450 nm (DAPI), 505 and 550 nm (GFP), 550 and 580 nm (YFP), 590 and 640 nm (mCherry/PI/FM4-64). The data relating to the image has been carried out using Image J.

Yeast Two-Hybrid Assays.

Yeast two-hybrid screening was performed using the SCAR2 as a bait, and the cDNA libraries were made with oligo dT and random oligo primers, using RNA from *Arabidopsis* whole tissue, and cloned in the pGADT7-rec plasmid (Clontech). The procedures of cDNA library generation and screening were described previously (60). The plasmid DNA from positive colonies were isolated and sequenced (Supplemental Table 1). For the direct yeast two-hybrid assay, a pair of bait and prey constructs (described above) were co-transformed into yeast strain AH109 and spotted onto a vector-selective medium lacking Trp and Leu (SD/-2) at 30 ℃ for 3 days. The yeast transformants were screened on the selective medium lacking Trp-Leu-His-Ade (SD/-4).

Protein purification and *in vitro* pull-down assay

The vector construction for the expression of proteins has been introduced above. The constructs were transformed in the *Escherichia coli* strain BL21 (DE3), and their protein expressions were induced by 250 μm/L isopropyl-b-D-thiogalactoside (IPTG). The MBP, MBP-VAP27-1, MBP-VAP27-1^{N} and MBP-VAP27-1^{A} proteins were purified with an amylose resin (NEB), and the GST, GST-SCAR2 (a.a. 1-432) and GST-SCAR2-LIP1 proteins were purified with GST Bind Resin (Novagen). For the protein interaction assay, the purified protein was incubated with resin-bound tagged fusion proteins for 2 h at 4°C with rotation in the binding buffer (50 mM Tris-HCl pH 7.5, 0.6% Triton X-100, 100 mM NaCl, and 1 × PMSF). The pellets were washed 5 times, eluted in SDS loading buffer, and boiled at 95°C for 10 min before immunoblot. The samples were resolved by SDS-PAGE and immunoblotted using an anti-MBP antibody (1:3000 dilution).

Light microscopy and 5-ethynyl-20-deoxyuridine (EdU) staining

Arabidopsis seedlings of Col-0, *scar1234*, and *vap27-1346* were germinated on 1/2 MS solid medium at 7 dpg. The cells in the cotyledon pavement were imaged using PI staining and quantified using the PaCeQuant plug-in to Image J (61). For the trichome

observation, various *Arabidopsis* lines were germinated on 1/2 MS solid medium at 10 dpg, and the roseate leaves were taken images by a Leica M205 FA dissecting scope.

To study the cytokinesis activity in root meristems, 2-day-old seedlings grown on 1/2 MS solid medium were transferred to 1/2 MS liquid medium containing 10 mM EdU (Life Technologies) for 6 h. Seedlings were then fixed for 1 h in freshly prepared fixative containing 3.7% (v/v) paraformaldehyde, 1% (v/v) Triton-X-100, and PBS, washed twice with 3% (w/v) bovine serum albumin (BSA) in PBS. Seedlings were then incubated with 1 ml Click-iT reaction mix (Click-iT EdU Image Kit, Life Technologies) containing 100 µl Click-iT reaction buffer, 800 µl CuSO4, 100 µl reaction buffer containing Alexa Fluor 594 for 1 h at room temperature under dark. The stained seedlings were then washed once with 3% (w/v) BSA in PBS solution and then labelled with 10 mg/ml DAPI in 3% PBS solution and kept in the dark before imaging. The ratio of EdU and DAPI labelled was analysed by confocal microscopy (Leica SP8). For the EdU-labelled nucleus visualisation, samples were excited with a 552 nm laser, and emission was collected through the 590-640 nm filters. DAPI was excited with a 405 nm laser line and visualised at the emission spectrum at 410-450 nm.

Election Microscopy

Three-day-old seedlings were selected, and their meristem region (about 2 mm from the tips) was prefixed in 2.5% glutaraldehyde (v/v in 0.1 M phosphate buffer, pH 7.2) for 2 h and then rinsed 3 times with 0.1 M phosphate buffer (pH 7.2). They were post-fixed in 1% OsO4 for 2 h, followed by three 15-minute rinses with 0.1 M phosphate buffer. Afterwards, the samples were dehydrated through an acetone series (30, 50, 70, 90, 100, 100, and 100%, v/v in ddH_2O) at room temperature. Then, the samples were infiltrated in a series of acetone/SPI-PON 812 resin mixtures (3:1, 1:1, 1:3, v/v) for 12 h per step and finally left in 100% SPI-PON 812 resin (SPI Supplies, West Chester). Samples were embedded in SPI-PON812 resin and polymerised at 60°C for 48 h. Ultrathin sections (70 nm) were prepared on an ultramicrotome (Leica EM UC7, Germany) with a diamond knife and collected on Formvar-coated grids. To enhance the

image contrast, the sections were stained with 2% uranyl acetate and lead citrate. Finally, the cell ultrastructure was observed using transmission electron microscopy (Hitachi H-7650, Tokyo, Japan).

Serial-Block Face Scanning Electron Microscopy and Data Reconstructions

Arabidopsis seeds were stratified at 4°C for 2 days, and seedlings grown to 10 days old. Root tissue was fixed overnight at 4°C in a solution of 2.5% glutaraldehyde, 2% formaldehyde, 2% sucrose, 2 mM $CaCl_2$, and Brij 35 in 0.1 M sodium cacodylate buffer (pH 7.2-7.3). Samples were then washed in the same 0.1 M sodium cacodylate buffer and incubated in 1% OsO_4 and 1.5% potassium ferricyanide for 1h in the dark at 4°C. Samples were washed 3 times in ddH_2O before incubation in 1% thiocarbohydrazide in ddH_2O before being washed again. A second osmium step was then performed, and samples were incubated in 2% OsO_4 in ddH_2O for 30 minutes with gentle agitation in the dark, followed by another washing step and overnight incubation at 4°C in 0.5% UA in ddH_2O. After another washing step, samples underwent a dehydration series of 10-minute washes in 10%, 20%, 30%, 50%, 70%, 90%, 100% and absolute ethanol × 2, respectively. Finally, samples were infiltrated with TAAB 812 Hard resin (T030) of increasing concentrations (3:1 Absolute ethanol: Resin, 1:1 Absolute ethanol: Resin and 1:3 Absolute ethanol: Resin, before 4 changes of 100% resin. Samples in resin were polymerised for 48h at 60°C.

The tips of resin blocks containing root tissue were trimmed and mounted onto aluminium pins with conductive epoxy glue and silver dag. Sputter coated with a 10-13 nm layer of gold using an Agar Auto Sputter Coater (Agar). A Merlin VP compact high-resolution scanning electron microscope (Zeiss) equipped with a 3View 2XP stage, an OnPoint back-scattered electron detector (Gatan-Ametek), and a focal charge compensation device (Zeiss) were used for imaging. The following conditions were used for image capture: 1.8 kV accelerating voltage, 30 μm aperture, high vacuum, 100% focal charge compensation, 5 nm pixel size, 50 nm section thickness, 1 μs pixel

time and an image size of 15000 × 15000 pixels. Data was processed using the IMOD software package. Cell plates were manually segmented as individual objects, and ER was segmented using the isosurface function as multiple objects in 3DMOD.

Latrunculin B treatment

For Latrunculin B treatment, seedlings were germinated on 1/2 MS solid medium at 2 dpg and transferred to 1/2 MS liquid medium with DMSO or 200 nM Lat B for 1 h, respectively. More than 10 single cells from each genotype were observed and measured.

Statistical analysis

All statistical graphics were performed using GraphPad Prism software (ver. 9.00). Results were compared, and data were expressed as mean ± SEM (Standard Error of Mean) for each symbol using appropriate statistical analysis methods (Student's t-test, one-way ANOVA or two-way ANOVA for multiple comparisons). P value < 0.05 was considered significant.

Acknowledgements

We thank the support from microscopy core facilities of the College of Horticulture and Forestry Sciences, Huazhong Agricultural University. The project was supported by NSFC grants (92254307, 32261160371), Fundamental Research Funds for the Central Universities (2662023PY011), Young Scientist Fostering Funds for the National Key Laboratory for Germplasm Innovation and Utilization of Horticultural Crops (Horti-PY-2023-001) to PW and a BBSRC grant, BBC516601/1, to PJH. We thank the support from microscopy core facilities of the College of Horticulture & Forestry Sciences, Huazhong Agricultural University. We thank Prof. Elison B. Blancaflor and Dr. Sabrina Chin (Noble Research Institute) for sharing the SCAR2-mCherry transgenic lines and the *scar1234* mutant. We thank Dr Weibing Yang (CEMPS) for the pUBQ:

GFP-Lifeact transgenic line. We thank Dr. Patrick Duckney (Durham University) and Dr. Tong Zhang (HZAU) for their help and advice throughout the project.

References

1. T. D. Pollard, Regulation of actin filament assembly by Arp2/3 complex and formins. *Annu Rev Biophys Biomol Struct* **36**, 451-477 (2007).
2. L. Xu, L. Cao, J. Li, C. J. Staiger, Cooperative actin filament nucleation by the Arp2/3 complex and formins maintains the homeostatic cortical array in Arabidopsis epidermal cells. *Plant Cell* **36**, 764-789 (2024).
3. M. Frank *et al.*, Activation of Arp2/3 complex-dependent actin polymerization by plant proteins distantly related to Scar/WAVE. *Proc Natl Acad Sci U S A* **101**, 16379-16384 (2004).
4. C. Zhang *et al.*, Arabidopsis SCARs function interchangeably to meet actin-related protein 2/3 activation thresholds during morphogenesis. *Plant Cell* **20**, 995-1011 (2008).
5. J. F. Uhrig *et al.*, The role of Arabidopsis SCAR genes in ARP2-ARP3-dependent cell morphogenesis. *Development* **134**, 967-977 (2007).
6. S. Chin *et al.*, Spatial and temporal localization of SPIRRIG and WAVE/SCAR reveal roles for these proteins in actin-mediated root hair development. *Plant Cell* **33**, 2131-2148 (2021).
7. C. Liu *et al.*, An actin remodeling role for Arabidopsis processing bodies revealed by their proximity interactome. *Embo j* **42**, e111885 (2023).
8. M. R. Facette *et al.*, The SCAR/WAVE complex polarizes PAN receptors and promotes division asymmetry in maize. *Nat Plants* **1**, 14024 (2015).
9. C. Zhang *et al.*, The endoplasmic reticulum is a reservoir for WAVE/SCAR regulatory complex signaling in the Arabidopsis leaf. *Plant Physiol* **162**, 689-706 (2013).
10. M. Yanagisawa, C. Zhang, D. B. Szymanski, ARP2/3-dependent growth in the plant kingdom: SCARs for life. *Front Plant Sci* **4**, 166 (2013).
11. J. Dyachok *et al.*, SCAR mediates light-induced root elongation in Arabidopsis through photoreceptors and proteasomes. *Plant Cell* **23**, 3610-3626 (2011).
12. P. Wang, C. Richardson, C. Hawes, P. J. Hussey, Arabidopsis NAP1 Regulates the Formation of Autophagosomes. *Curr Biol* **26**, 2060-2069 (2016).
13. J. Martinek *et al.*, ARP2/3 complex associates with peroxisomes to participate in pexophagy in plants. *Nat Plants* **9**, 1874-1889 (2023).
14. C. Pain, F. Tolmie, S. Wojcik, P. Wang, V. Kriechbaumer, intER-ACTINg: The structure and dynamics of ER and actin are interlinked. *J Microsc* **291**, 105-118 (2023).
15. J. Zang, V. Kriechbaumer, P. Wang, Plant cytoskeletons and the endoplasmic reticulum network organization. *J Plant Physiol* **264**, 153473 (2021).
16. P. Wang, T. J. Hawkins, P. J. Hussey, Connecting membranes to the actin cytoskeleton. *Curr Opin Plant Biol* **40**, 71-76 (2017).
17. P. Cao, L. Renna, G. Stefano, F. Brandizzi, SYP73 Anchors the ER to the Actin Cytoskeleton for Maintenance of ER Integrity and Streaming in Arabidopsis. *Curr Biol* **26**, 3245-3254 (2016).
18. P. Wang, P. J. Hussey, Interactions between plant endomembrane systems and the actin cytoskeleton. *Front Plant Sci* **6**, 422 (2015).
19. I. Sparkes, J. Runions, C. Hawes, L. Griffing, Movement and remodeling of the endoplasmic

reticulum in nondividing cells of tobacco leaves. *Plant Cell* **21**, 3937-3949 (2009).
20. P. Wang, C. Hawes, P. J. Hussey, Plant Endoplasmic Reticulum-Plasma Membrane Contact Sites. *Trends Plant Sci* **22**, 289-297 (2017).
21. S. Sun *et al.*, Stay in touch with the endoplasmic reticulum. *Sci China Life Sci* **67**, 230-257 (2024).
22. C. J. Loewen, T. P. Levine, A highly conserved binding site in vesicle-associated membrane protein-associated protein (VAP) for the FFAT motif of lipid-binding proteins. *J Biol Chem* **280**, 14097-14104 (2005).
23. K. Bürstenbinder *et al.*, Arabidopsis calmodulin-binding protein IQ67-domain 1 localizes to microtubules and interacts with kinesin light chain-related protein-1. *J Biol Chem* **288**, 1871-1882 (2013).
24. P. Wang *et al.*, The plant cytoskeleton, NET3C, and VAP27 mediate the link between the plasma membrane and endoplasmic reticulum. *Curr Biol* **24**, 1397-1405 (2014).
25. J. Zang *et al.*, A novel plant actin-microtubule bridging complex regulates cytoskeletal and ER structure at ER-PM contact sites. *Curr Biol* **31**, 1251-1260.e1254 (2021).
26. A. Smertenko *et al.*, Plant Cytokinesis: Terminology for Structures and Processes. *Trends Cell Biol* **27**, 885-894 (2017).
27. E. Lipka, A. Herrmann, S. Mueller, Mechanisms of plant cell division. *Wiley Interdiscip Rev Dev Biol* **4**, 391-405 (2015).
28. P. Du *et al.*, AtMAC stabilizes the phragmoplast by crosslinking microtubules and actin filaments during cytokinesis. *J Integr Plant Biol* **65**, 1950-1965 (2023).
29. H. Li *et al.*, Arabidopsis MAP65-4 plays a role in phragmoplast microtubule organization and marks the cortical cell division site. *New Phytol* **215**, 187-201 (2017).
30. P. Dahiya, K. Bürstenbinder, The making of a ring: Assembly and regulation of microtubule-associated proteins during preprophase band formation and division plane set-up. *Curr Opin Plant Biol* **73**, 102366 (2023).
31. A. Smertenko *et al.*, Phragmoplast microtubule dynamics - a game of zones. *J Cell Sci* **131** (2018).
32. M. Abu-Abied *et al.*, Myosin XI-K is involved in root organogenesis, polar auxin transport, and cell division. *J Exp Bot* **69**, 2869-2881 (2018).
33. C. H. Huang, F. L. Peng, Y. J. Lee, B. Liu, The microtubular preprophase band recruits Myosin XI to the cortical division site to guide phragmoplast expansion during plant cytokinesis. *Dev Cell* 10.1016/j.devcel.2024.05.015 (2024).
34. S. Z. Wu, M. Bezanilla, Myosin VIII associates with microtubule ends and together with actin plays a role in guiding plant cell division. *Elife* **3** (2014).
35. C. R. Hawes, B. E. Juniper, J. C. Horne, Low and high voltage electron microscopy of mitosis and cytokinesis in maize roots. *Planta* **152**, 397-407 (1981).
36. J. M. Seguí-Simarro, J. R. Austin, 2nd, E. A. White, L. A. Staehelin, Electron tomographic analysis of somatic cell plate formation in meristematic cells of Arabidopsis preserved by high-pressure freezing. *Plant Cell* **16**, 836-856 (2004).
37. K. Knox *et al.*, Putting the Squeeze on Plasmodesmata: A Role for Reticulons in Primary Plasmodesmata Formation. *Plant Physiol* **168**, 1563-1572 (2015).
38. Z. P. Li *et al.*, Plant plasmodesmata bridges form through ER-dependent incomplete cytokinesis. *Science* **386**, 538-545 (2024).

39. A. Nebenführ, J. A. Frohlick, L. A. Staehelin, Redistribution of Golgi stacks and other organelles during mitosis and cytokinesis in plant cells. *Plant Physiol* **124**, 135-151 (2000).
40. X. Cheng, M. Bezanilla, SABRE populates ER domains essential for cell plate maturation and cell expansion influencing cell and tissue patterning. *Elife* **10** (2021).
41. D. Zhang, T. C. Bidone, D. Vavylonis, ER-PM Contacts Define Actomyosin Kinetics for Proper Contractile Ring Assembly. *Curr Biol* **26**, 647-653 (2016).
42. T. Higaki, N. Kutsuna, T. Sano, S. Hasezawa, Quantitative analysis of changes in actin microfilament contribution to cell plate development in plant cytokinesis. *BMC Plant Biol* **8**, 80 (2008).
43. T. D. Pollard, J. A. Cooper, Actin, a central player in cell shape and movement. *Science* **326**, 1208-1212 (2009).
44. M. J. Deeks, P. J. Hussey, Arp2/3 and SCAR: plants move to the fore. *Nat Rev Mol Cell Biol* **6**, 954-964 (2005).
45. P. Wang *et al.*, Plant VAP27 proteins: domain characterization, intracellular localization and role in plant development. *New Phytol* **210**, 1311-1326 (2016).
46. J. Dyachok *et al.*, Plasma membrane-associated SCAR complex subunits promote cortical F-actin accumulation and normal growth characteristics in Arabidopsis roots. *Mol Plant* **1**, 990-1006 (2008).
47. C. Li *et al.*, TraB family proteins are components of ER-mitochondrial contact sites and regulate ER-mitochondrial interactions and mitophagy. *Nat Commun* **13**, 5658 (2022).
48. E. Lee *et al.*, Ionic stress enhances ER-PM connectivity via phosphoinositide-associated SYT1 contact site expansion in Arabidopsis. *Proc Natl Acad Sci U S A* **116**, 1420-1429 (2019).
49. B. K. Nelson, X. Cai, A. Nebenführ, A multicolored set of in vivo organelle markers for co-localization studies in Arabidopsis and other plants. *Plant J* **51**, 1126-1136 (2007).
50. M. Takeuchi *et al.*, Single microfilaments mediate the early steps of microtubule bundling during preprophase band formation in onion cotyledon epidermal cells. *Mol Biol Cell* **27**, 1809-1820 (2016).
51. C. M. McMichael, S. Y. Bednarek, Cytoskeletal and membrane dynamics during higher plant cytokinesis. *New Phytol* **197**, 1039-1057 (2013).
52. P. Liu, M. Qi, X. Xue, H. Ren, Dynamics and functions of the actin cytoskeleton during the plant cell cycle. *Chinese Science Bulletin* **56**, 3504-3510 (2011).
53. A. Lebecq, A. Fangain, A. Boussaroque, M. C. Caillaud, Dynamic apico-basal enrichment of the F-actin during cytokinesis in Arabidopsis cells embedded in their tissues. *Quant Plant Biol* **3**, e4 (2022).
54. A. M. Monzon, A. Hatos, M. Necci, D. Piovesan, S. C. E. Tosatto, Exploring Protein Intrinsic Disorder with MobiDB. *Methods Mol Biol* **2141**, 127-143 (2020).
55. S. E. Murphy, T. P. Levine, VAP, a Versatile Access Point for the Endoplasmic Reticulum: Review and analysis of FFAT-like motifs in the VAPome. *Biochim Biophys Acta* **1861**, 952-961 (2016).
56. J. A. Slee, T. P. Levine, Systematic prediction of FFAT motifs across eukaryote proteomes identifies nucleolar and eisosome proteins with the predicted capacity to form bridges to the endoplasmic reticulum. *Contact (Thousand Oaks)* **2**, 1-21 (2019).
57. I. Karahara, L. A. Staehelin, Y. Mineyuki, A role of endocytosis in plant cytokinesis. *Commun Integr Biol* **3**, 36-38 (2010).

58. C. G. Rasmussen, M. Bellinger, An overview of plant division-plane orientation. *New Phytol* **219**, 505-512 (2018).
59. H. Buschmann, S. Müller, Update on plant cytokinesis: rule and divide. *Curr Opin Plant Biol* **52**, 97-105 (2019).
60. L. Camacho, A. P. Smertenko, J. Pérez-Gómez, P. J. Hussey, I. Moore, Arabidopsis Rab-E GTPases exhibit a novel interaction with a plasma-membrane phosphatidylinositol-4-phosphate 5-kinase. *J Cell Sci* **122**, 4383-4392 (2009).
61. B. Möller, Y. Poeschl, R. Plötner, K. Bürstenbinder, PaCeQuant: A Tool for High-Throughput Quantification of Pavement Cell Shape Characteristics. *Plant Physiol* **175**, 998-1017 (2017).

Figures and Tables

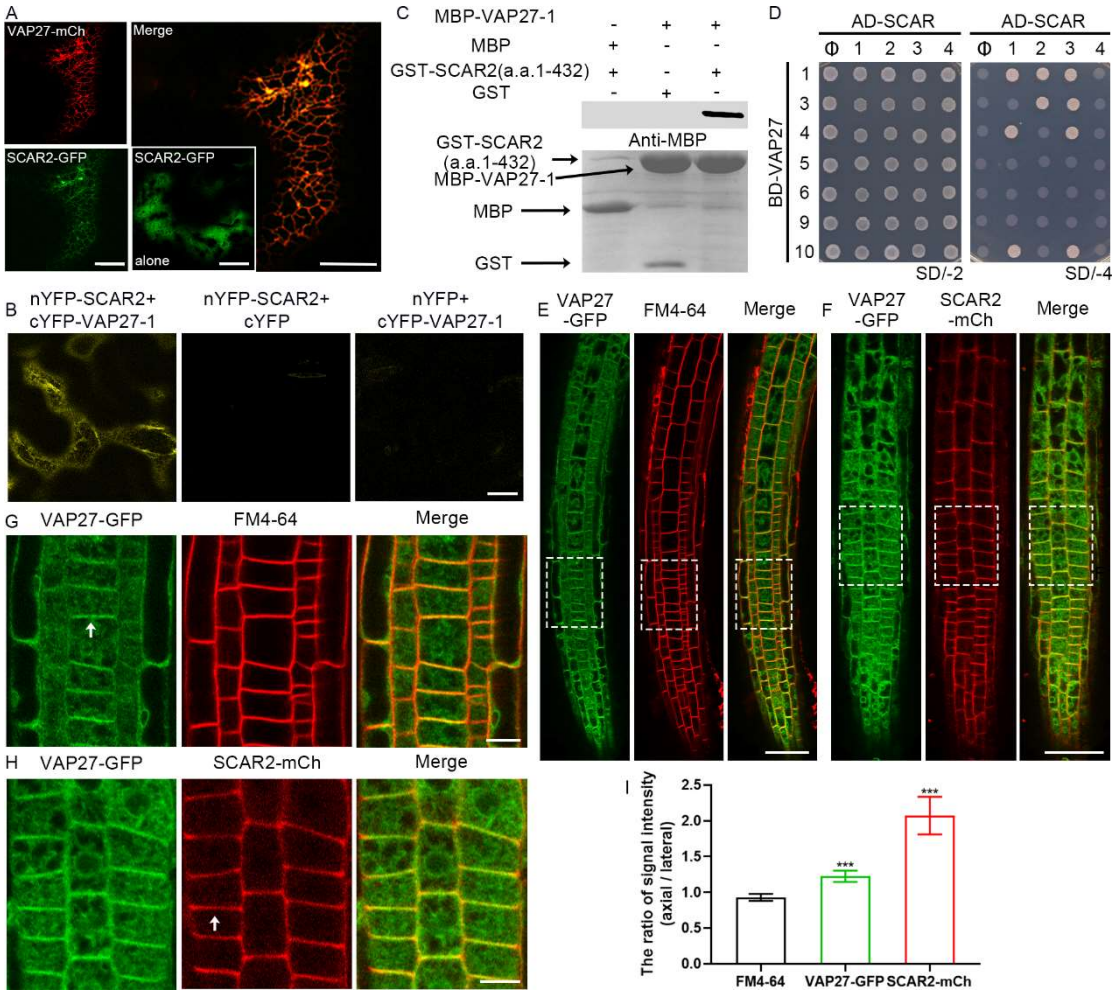

Figure 1. SCAR2 interacts with VAP27 proteins and exhibits polarised localisation at the transverse cell plate. (A) In *N. benthamiana* leaf epidermal cells, VAP27-mCh recruits GFP-SCAR2 to the ER membrane when co-expressed. Scale bars, 20 μm. **(B)** BiFC assays in *N. benthamiana* show that SCAR2 interacts with VAP27-1 on the ER. An empty vector is used as a negative control. Scale bars, 20 μm. **(C)** *In vitro* pull-down assay confirmed the interaction between MBP-VAP27-1 and a GST-SCAR2 truncation. The top panel shows the pull-down results, where VAP27-1 is detected in the presence of GST-SCAR2 (a.a. 1-432) using an anti-MBP antibody; the bottom panel shows the total protein stained by Coomassie brilliant blue. MBP protein and GST protein were used as negative controls (left and middle lanes). Arrows indicate specific bands of purified proteins. **(D)** A one-on-one yeast two-hybrid screen revealed conserved interactions between the SCAR and VAP27 families. Transformed yeast cells were cultured on SD/-Trp-Leu (SD/-2) or SD/-Trp-Leu-His-Ade (SD/-4) medium, respectively. **(E-H)** VAP27-GFP co-localized with FM4-64 and SCAR2-mCh in transgenic *Arabidopsis* roots at the transverse cell interface (arrows). Scale bars, 50 μm in (E-F) and 10 μm in (G-H). The signal intensity of FM4-64, VAP27 and SCAR2 at

713 the axial/lateral cell membrane was quantified as in (I). Quantification was performed
714 using at least 30 cells from 5 roots. Two-tailed t-test, ***$p < 0.001$.

715

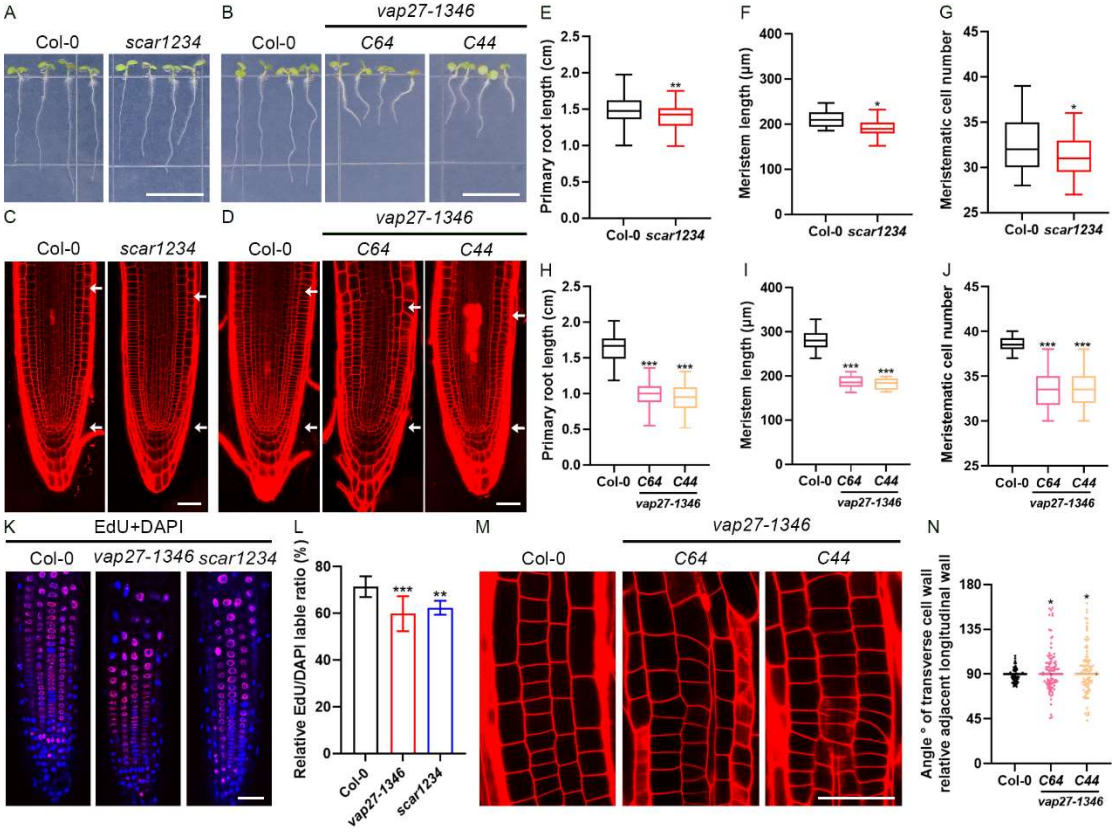

Figure 2. The quadruple mutant of *vap27-1346* and *scar1234* exhibit root growth defects. (A-D) Images of Col-0, *scar1234,* and *vap27-1346* seedlings (5 dpg) indicate that the mutation of SCAR and VAP27 resulted in similar root defects. Roots were stained with PI and imaged at 5 dpg. White arrows indicate the quiescent centre (QC) and root meristem boundary. **(E-J)** Quantifications of the primary root length, root meristem length and meristematic cell number of seedlings in (A-D). Scale bars, 1 cm in (A and B), and for each dataset, n >50. Scale bars, 50 μm in (C and D), n ≥ 10 roots. Student's t-test, *p < 0.05, **p < 0.01, ***p < 0.001. **(K-L)** The EdU and DAPI staining reveals that *vap27-1346* and *scar1234* exhibit cell division defects. Scale bars, 50 μm. The percentage of EdU labelled nuclei in root meristem was quantified in Col-0, *scar1234* and *vap27-1346* (as in L). n ≥ 10, two-tailed t test, *p < 0.05, **p < 0.01, ***p < 0.001. **(M-N)** The organisation of root epidermal cells is more disordered in the *vap27-1346* mutant, as indicated by the angles of the transverse cell plates, which show higher variability in the VAP27 mutant. Roots were stained with PI and imaged at 5 dpg. Scale bars, 50 μm. For each data set, n = 100, two-tailed t-test, *p < 0.05.

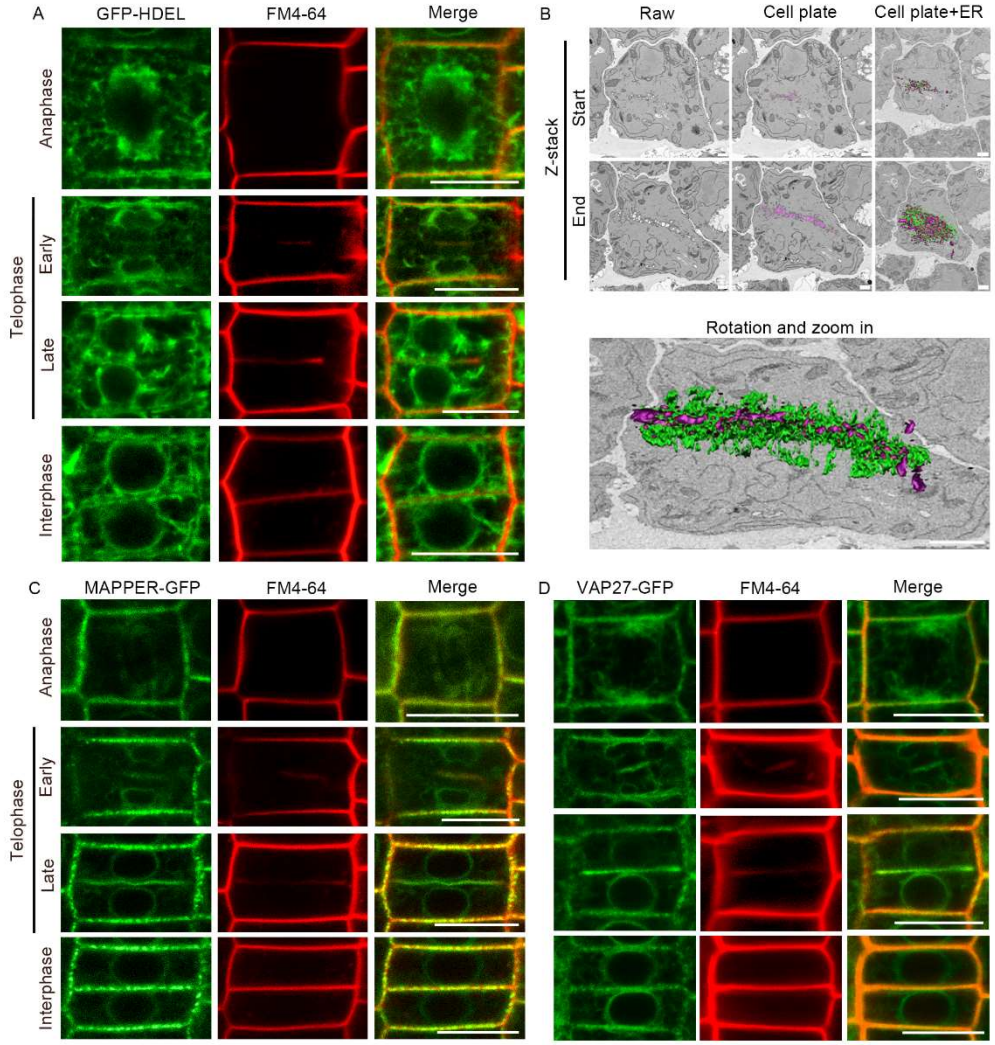

733

734 **Figure 3. ER membrane and ER-PM tethering proteins are enriched at the cell**
735 **plate. (A)** The ER network (GFP-HDEL labelled) is enriched at the cell division plane
736 at different stages. Scale bars, 10 μm. **(B)** SBEM images of a dividing cell from
737 *Arabidopsis* root meristem. The ER membrane is green, and the cell plate/tubular
738 network is magenta. Scale bars, 2 μm. **(C-D)** ER-PM tethering proteins (MAPPER-
739 GFP, VAP27-GFP) exhibit polarised localisation at the cell plate/division plane. FM4-
740 64 is used to label PM and cell plate membranes during cytokinesis. Scale bars, 10 μm.

741

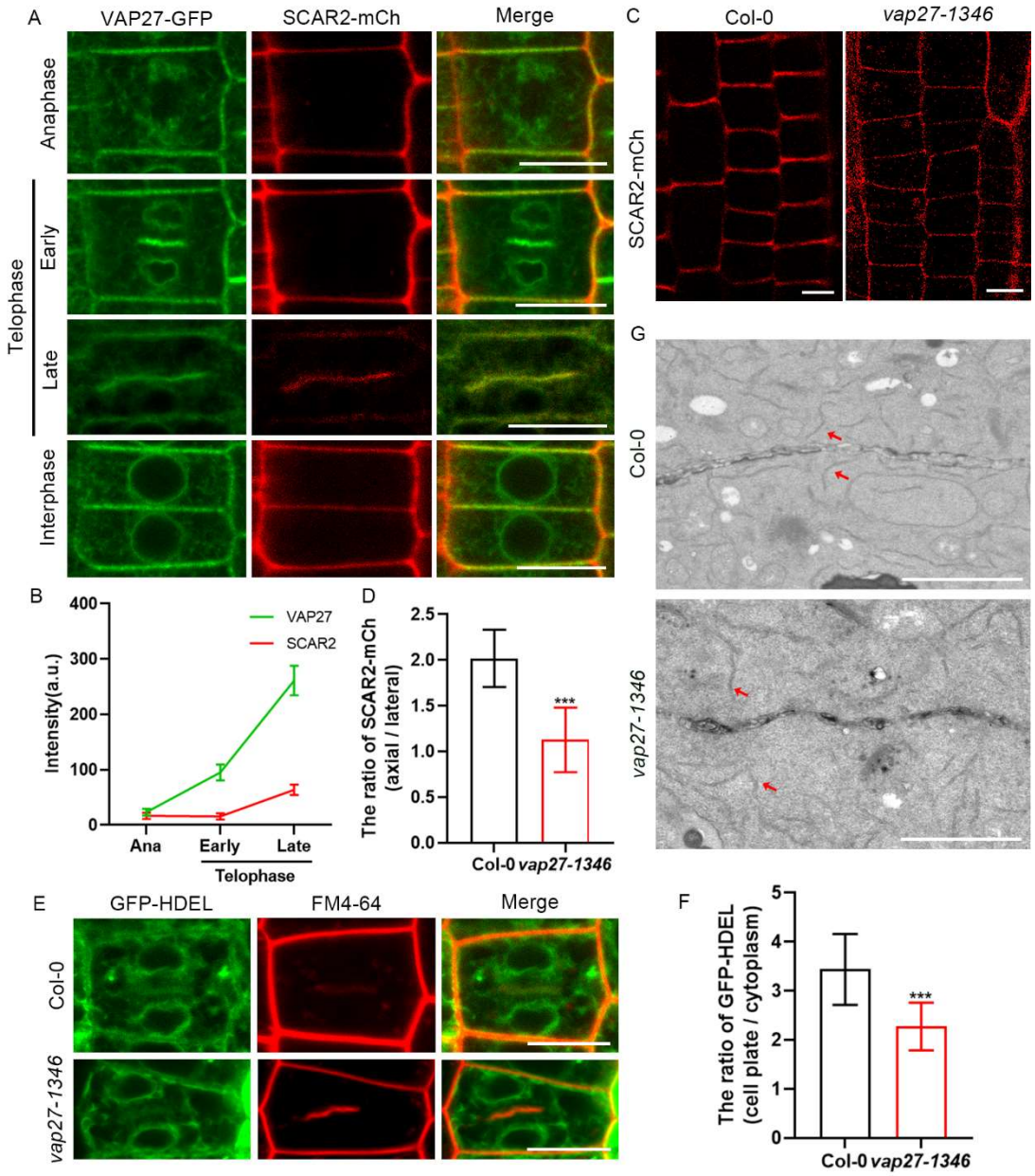

Figure 4. VAP27 regulates the accumulation of SCAR2 and ER membrane to the division plane. (A-B) Cells from transgenic *Arabidopsis* root meristem expressing VAP27-GFP and SCAR2-mCh. Both fusion proteins are recruited to the cell plate, and the transverse cell junctions during cytokinesis, but the recruitment of VAP27 appears earlier than SCAR2. Please note that VAP27 and SCAR2 are enriched at the cell plate edge (arrows). The relative signal intensity (signals from cell plate/cytoplasm) of VAP27-GFP and SCAR2-mCh at the early and late telophase was quantified in (B). Scale bars, 10 μm. At least 10 cells were analysed per stage. **(C)** The localisation of SCAR2-mCh in root meristem cells is affected in the *vap27-1346* mutant. Scale bars, 10 μm. **(D)** The quantification of SCAR2-mCh signals at the axial/lateral cell membrane of the Col-0 and *vap27-1346* mutant, polarised localisation of SCAR2 at the transverse cell junctions is perturbed in the absence of VAP27. n > 30, two-tailed t-test,

***P < 0.01. **(E-F)** Images of transgenic *Arabidopsis* root meristem cells expressing GFP-HDEL; signals of the ER membrane at the division plane (late-telophase) are reduced significantly in the *vap27-1346* mutant. The ratios of the ER labelling at the cell division plane and cytoplasm are shown in (E). FM4-64 is used to label cell membranes. Scale bars, 10 μm. At least 10 cells were analysed for each stage. **(G)** TEM images suggest that the ER membranes at the cell plate region are reduced in *vap27-1346* mutant at 3 dpg. Scale bars, 2 μm.

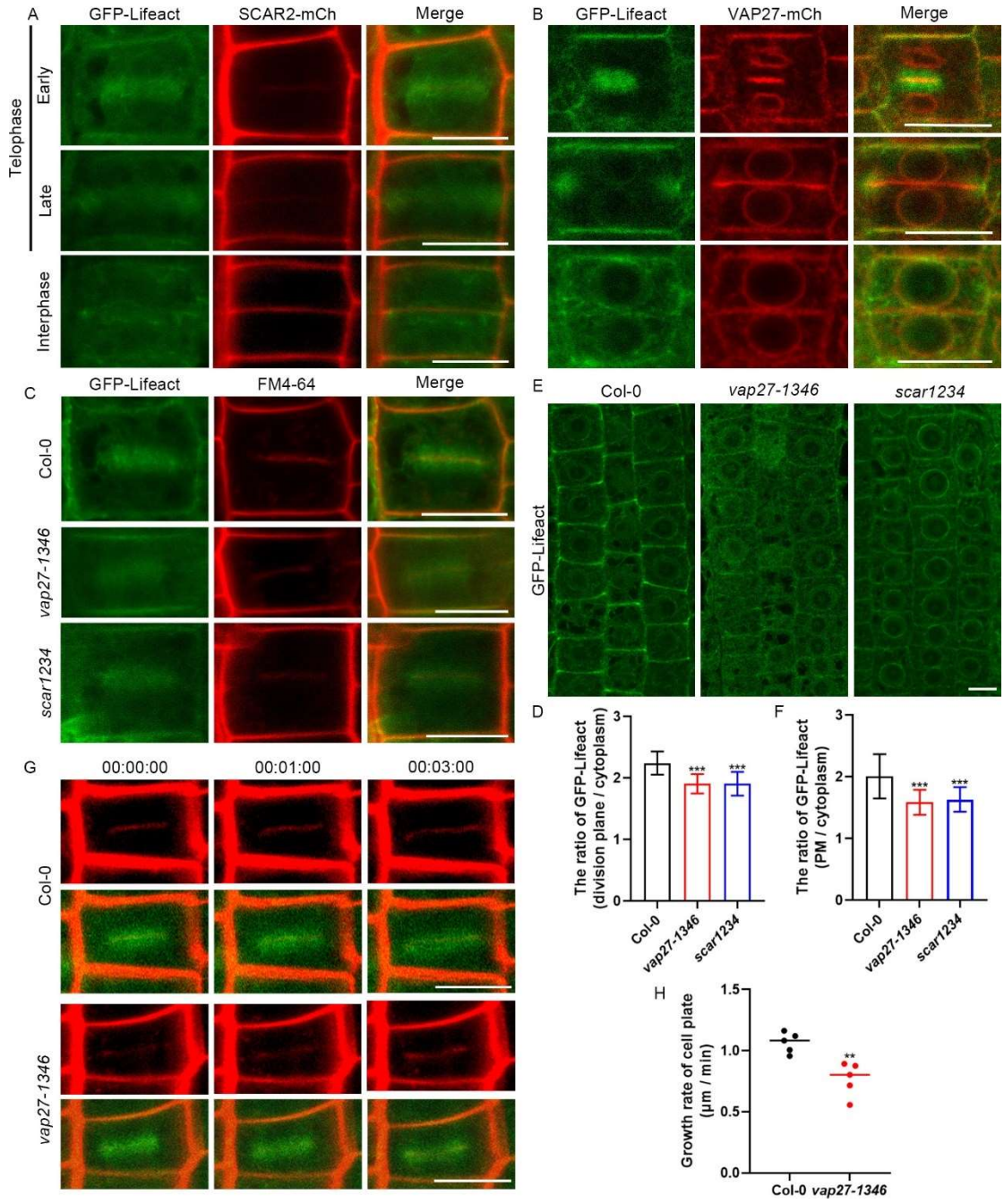

762

763 **Figure 5. VAP27 and SCAR2 proteins regulate actin accumulation at the division**
764 **plane and transverse cell interface. (A-B)** In *Arabidopsis* root meristem cells, GFP-
765 Lifeact labelled actin filaments form actin patches and co-localize with SCAR2-mCh
766 or VAP27-mCh labelled cell plates. Scale bars, 10 μm. **(C-D)** Images of transgenic
767 *Arabidopsis* root meristem cells expressing GFP-Lifeact, signals of the actin filaments
768 at the division plane (late-telophase) are reduced significantly in the *vap27-1346*
769 mutant. The ratios of the actin labelling at the cell division plane and cytoplasm are
770 shown in (D). FM4-64 is used to label cell plates. Scale bars, 10 μm. At least 10 cells
771 were analysed for each stage. **(E-F)** Images of transgenic *Arabidopsis* root epidermal
772 cells expressing GFP-Lifeact, signals of the actin filaments at the transverse cell

interface are reduced significantly in the *vap27-1346* and *scar1234* mutant. **(G-H)** Time-series imaging reflected a significantly slower growth rate of the cell plate in the *vap27-1346* mutant than in the wild type. FM4-64 is used to label cell plates. Actin filements are labelled with green fluorescence. Scale bars, 10 μm. Cell plates with an initial length at 7-8 μm were selected and imaged for three-minutes.

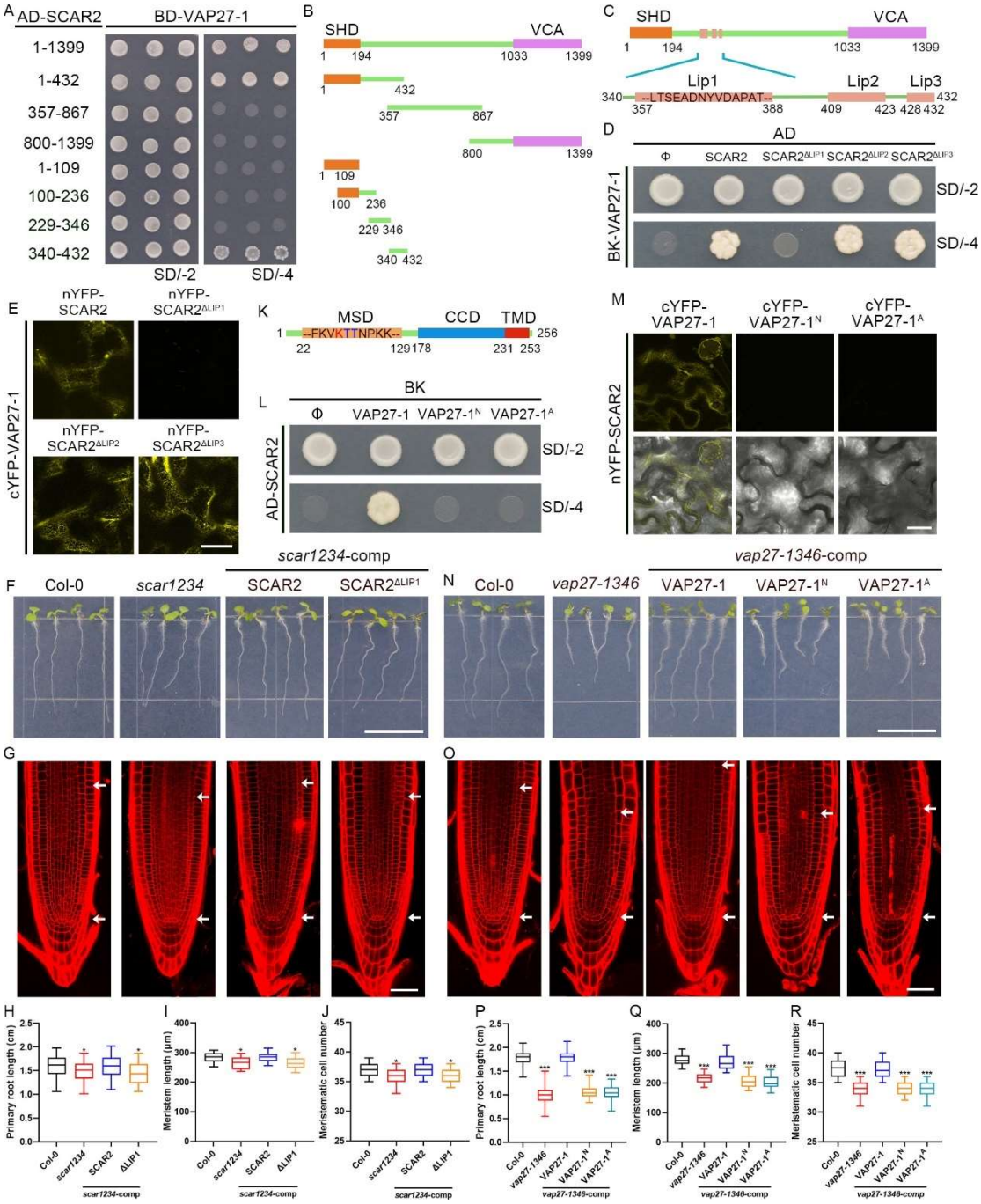

Figure 6. Functional complementation studies indicate the interaction between SCAR2 and VAP27-1 is essential for their function. (A-B) Yeast two-hybrid assay suggests the C-terminal sequence of SCAR2 (a.a. 340-432) is required for VAP27 interaction. **(C)** Three predicted linear interacting peptides (LIP) are found between a.a. 340-432 on SCAR2, and the LIP1 sequence contains an FFAT-like motif. **(D-E)** Y2H and BiFC assays show that SCAR2 without LIP1 sequence (SCAR2$^{\Delta LIP1}$) fails to interact with VAP27-1. Scale bars, 20 μm. **(F-G)** Gene complementation assay suggests that the expression of SCAR2$^{\Delta LIP1}$ (pSCAR2:SCAR2$^{\Delta LIP1}$-HA/*scar1234,* denoted as *scar1234-comp*$^{\Delta LIP1}$) cannot fully complement the root phenotype of the *scar1234* mutant, suggesting VAP27-1 interaction is important for SCAR2 function. **(H-J)**

Quantifications of primary root length, meristem length, and meristematic cell number in (F-G). **(K)** The conserved lysine (K) and Threonine (T) residues within the major sperm domain (MSD) are likely responsible for interacting with the FFAT motif. **(L-M)** Y2H and BiFC assays demonstrate that these conserved residues are critical for the interactions between SCAR2 and VAP27-1. Scale bars, 20 μm. **(N-O)** The expression of full-length VAP27-1 (pVAP27-1:VAP27-1-HA) complements root phenotypes of the *vap27-1346* mutant, while the VAP27-1^{N} (pVAP27-1:VAP27-1^{N}-HA) and VAP27-1^{A} (pVAP27-1:VAP27-1^{A}-HA) point mutant fails to complement the mutant phenotype. **(P-R)** Quantifications of primary root length, meristem length, and meristematic cell number in (N-O). Roots were stained with PI and imaged at 5 dpg. White arrows indicate the QC and root meristem boundary. Scale bars, 1 cm in (F and N) and 50 μm in (G and O), respectively. For each data set in (H and P), $n \geq 50$. For each data set in (I-J and Q-R), $n \geq 10$, two-tailed t-test, $^{*}p < 0.05$, $^{**}p < 0.01$, $^{***}p < 0.001$.

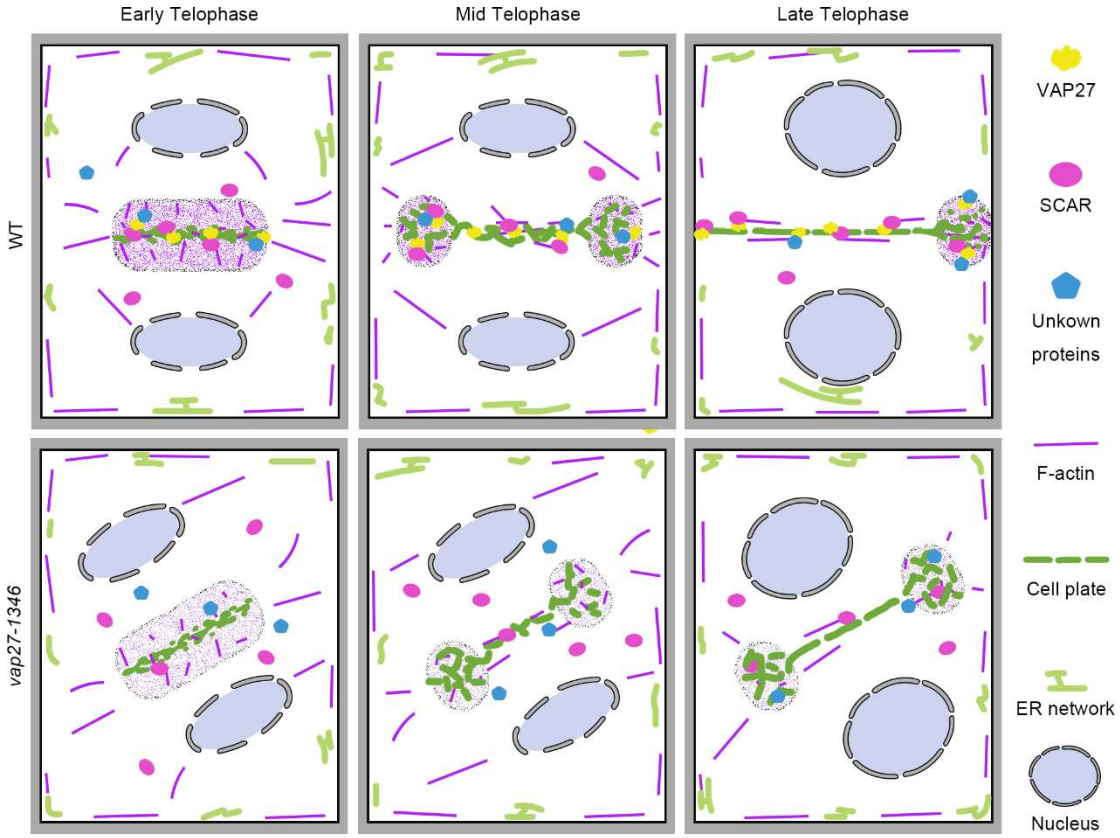

Figure 7. Schematic illustration of VAP27-SCAR regulated ER-PM-Actin interaction during cytokinesis. In wild-type cells, VAP27 is localised to the ER and ER-PM contact sites, and it is significantly enriched on the cell division plane. As the cell divides, VAP27 gradually accumulates at the cell plate region, where it recruits the SCAR/WAVE complex to promote actin nucleation and cell plate expansion. In the *vap27-1346* mutant, SCAR cannot be recruited to the cell plate to activate actin nucleation, resulting in abnormal cell plate expansion rate, orientation and assembly.

Supplemental Figures

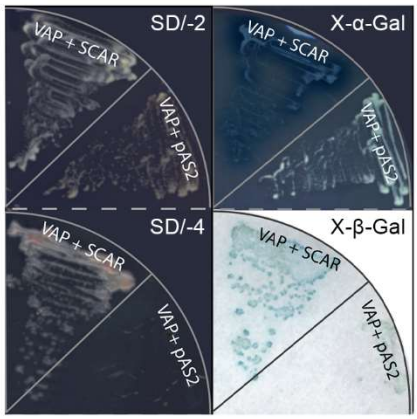

Figure S1. VAP27-1 was identified as a SCAR2 interacting protein from a yeast-two-hybrid screen. Transformed yeast cells were cultured on SD/-Trp-Leu (SD/-2), SD/-Trp-Leu-His-Ade (SD/-4) or SD/-4 medium supplemented with X-Gal, respectively.

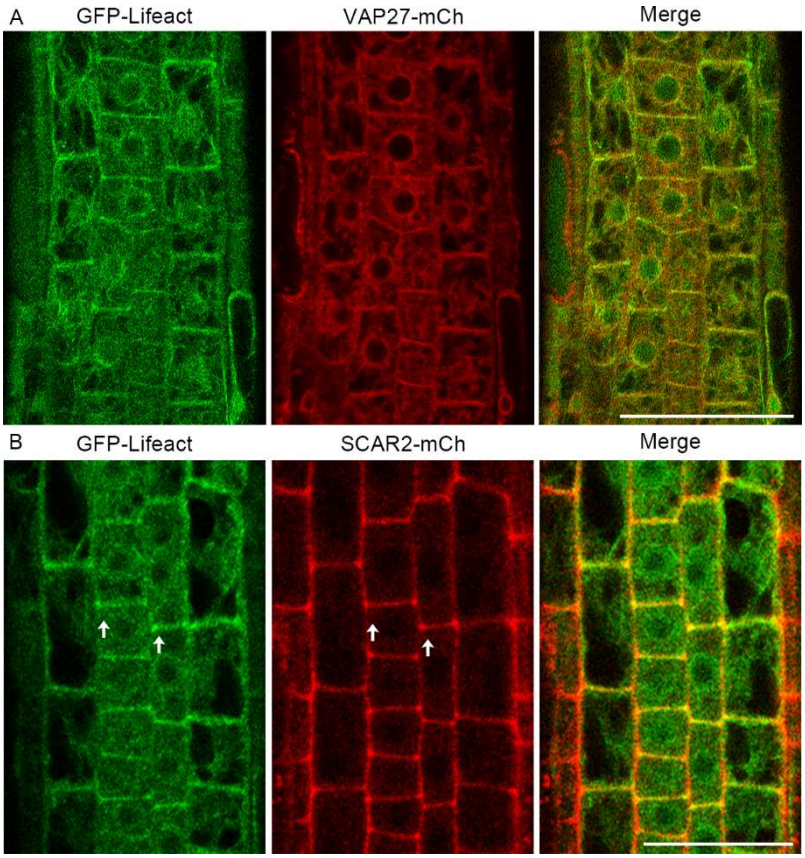

Figure S2. VAP27, SCAR2 and actin filaments are enriched at the transverse cell interface and corners. (A-B) Co-localisation of GFP-Lifeact with VAP27-mCh / SCAR2-mCh in *Arabidopsis* root epidermal cells. Arrows indicate the enrichment of Actin and SCAR2 at cell corners. Bars: 50 μm.

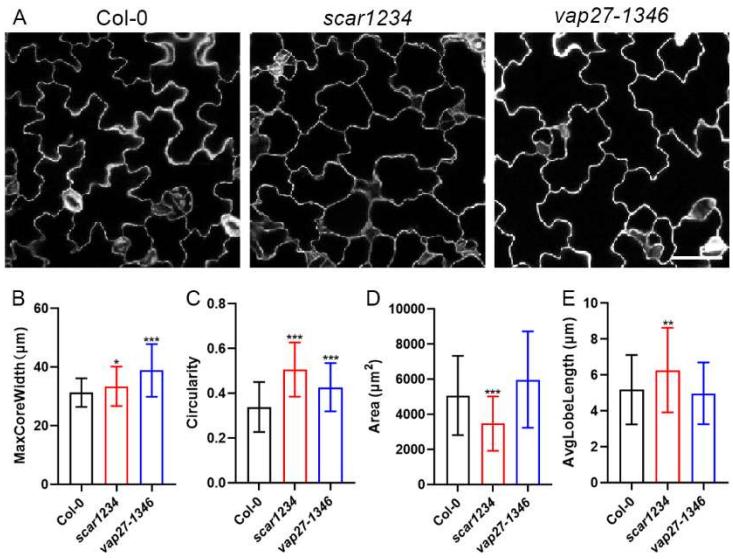

Figure S3. The quadruple mutant of *scar1234* and *vap27-1346* exhibit pavement cell morphogenesis defects. (A) Confocal images of cotyledon leaf pavement cells from Col-0, *scar1234* and *vap27-1346* mutants. Seedlings at 7 dpg were stained with 50 mM PI for observation. Scale bar, 50 μm. **(B-D)** Quantifications of cell circularity, cell area, lobe length, and maximum core width in different genetic backgrounds. Both *scar1234* and *vap27-1346* mutants show similar defects in cell circularity and the maximum core width. $n \geq 50$ (from at least 5 biological replicates), two-tailed t-test, *$p < 0.05$, **$p < 0.01$, ***$p < 0.001$.

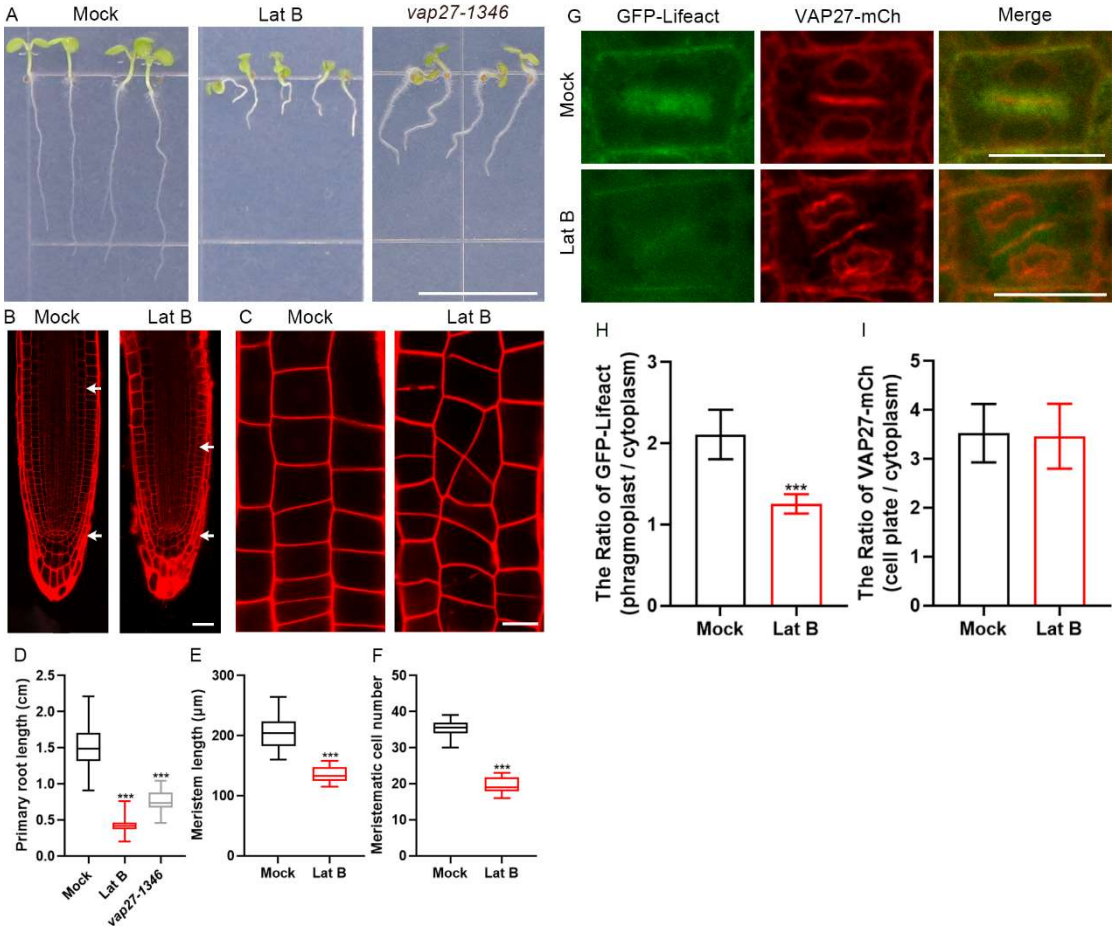

Figure S4. Actin depolymerisation mimics the root development phenotype of the *vap27-1346* mutant. (A-B) Low concentration Lat B treatment (150 nM) affects root development (at 5 dpg), leading to a phenotype similar to the *vap27-1346* mutant. White arrowheads indicate the QC and root meristem boundary. Scale bars, 1 cm in (A) and 50 μm in (B), respectively. **(C)** Cell organisation in root meristems is affected dramatically after Lat B treatment. Scale bars, 10 μm. **(D-F)** Quantifications of the primary root length, root meristem length and meristematic cell number in (A-B). For each data set in (A), $n \geq 50$. For each data set in (B), $n \geq 10$, two-tailed t-test, $*p < 0.05$, $**p < 0.01$, $***p < 0.001$. **(G)** In images of transgenic *Arabidopsis* root meristem cells expressing GFP-Lifeact and VAP27-mCh, the density of actin filaments at the division plane is reduced significantly after low-concentration Lat B treatment (200 nM). However, the signal of the ER membrane at the division plane is unaffected. Scale bars, 10 μm. At least 10 cells were analysed for mock and treated with Lat B. **(H-I)** The ratios of ER and actin signals at the cell division plane and cytoplasm are quantified (G).

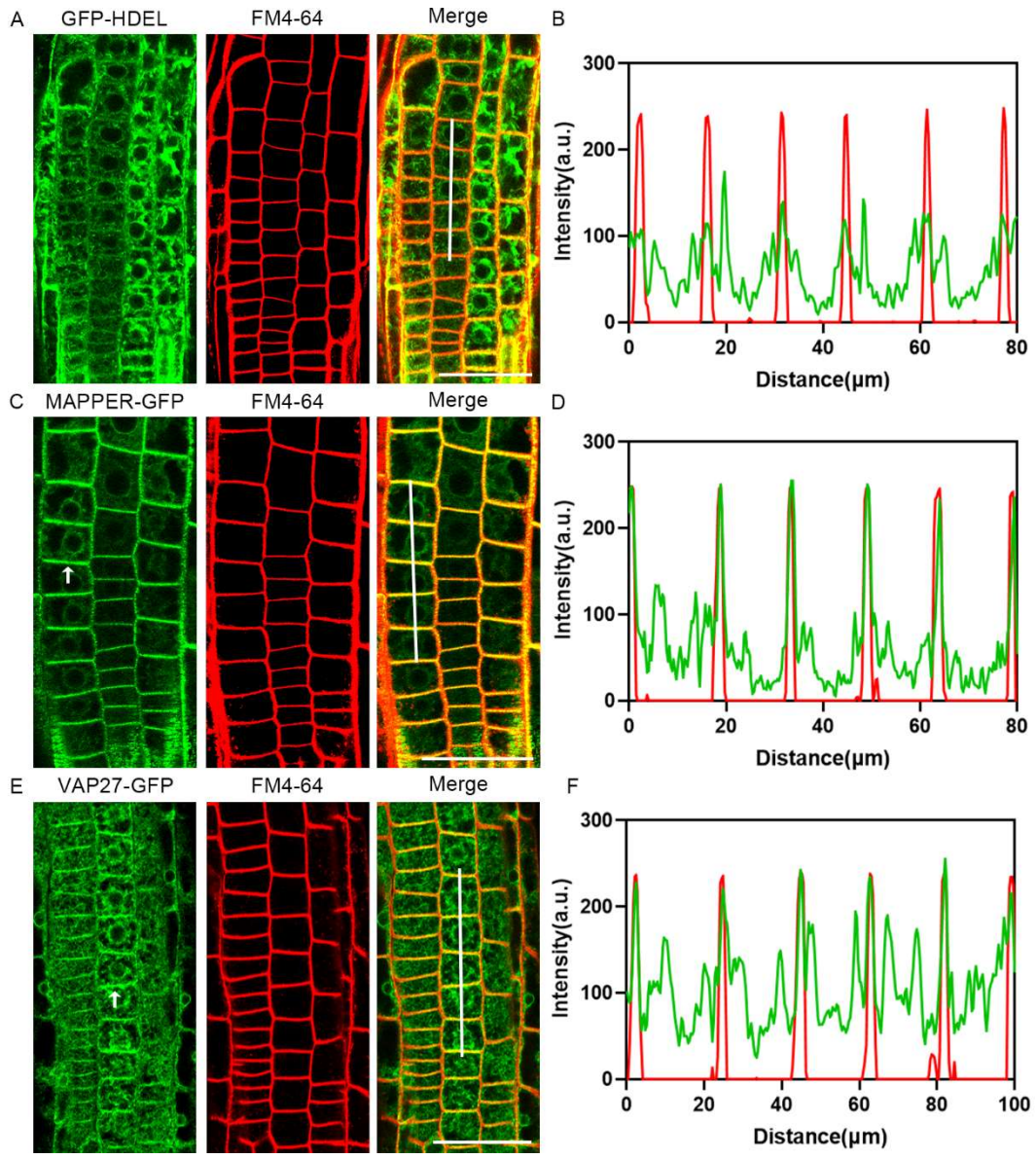

878

879 **Figure S5. ER-PM tethering proteins are enriched at the transverse cell junctions**
880 **of root meristem cells. (A, C, E)** Confocal images showing the localisation of GFP-
881 HDEL, MAPPER-GFP and VAP27-GFP in root meristems. FM4-64 is used to label
882 the PM. Please note MAPPER and VAP27 (both are known as ER-PM tethering
883 proteins) enrich at the transverse cell junction (arrows). Scale bars, 50 μm. **(B, D, F)**
884 Signal intensity along the lines is displayed graphically. The co-localisations between
885 FM4-64 and ER/ER-PM tethering proteins suggest the transverse cell junctions in root
886 meristem are abundant in ER-PM association.

887

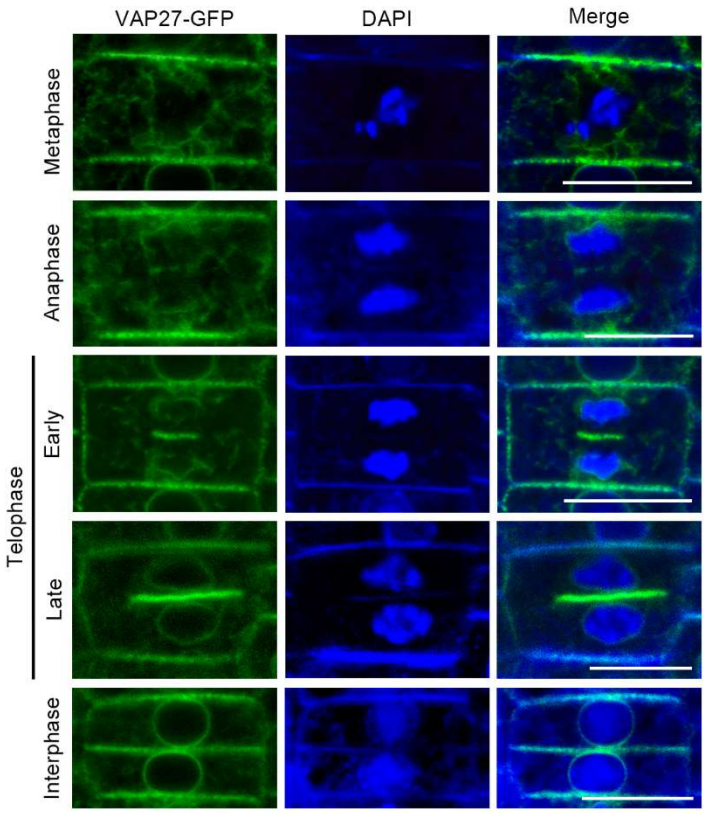

888 **Figure S6. The localisation of VAP27-GFP during cytokinesis.** Images of transgenic
889 *Arabidopsis* root meristem cells expressing VAP27-GFP, which is gradually
890 accumulated on the cell plate at the telophase. DAPI is used for nucleus staining. Scale
891 bars, 10 μm.

892

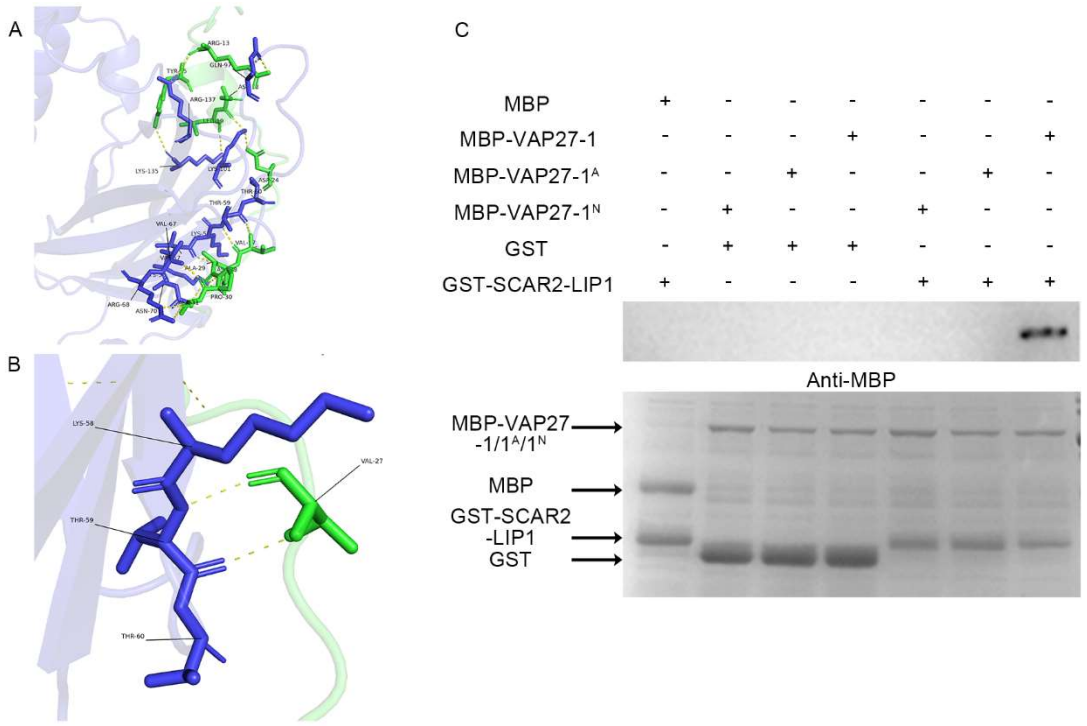

Figure S7. Verifications of VAP27-1 and SCAR2-LIP1 interaction using AlphaFold3 and *in vitro* pull-down assay. (A-B) The interaction is based on multiple interacting amino acid residues between the two proteins in (A). A hydrogen bond between the 59th amino acid threonine of VAP27-1 and the 27th amino acid valine of SCAR2-LIP1 is likely involved in protein interaction (B). The VAP27 protein is shown in blue, and the SCAR2-LIP1 peptide is shown in green. **(C)** *In vitro* pull-down assay confirmed the interaction between MBP-VAP27-1 and the GST-SCAR2-LIP1 truncation. The top panel shows the pull-down results, where VAP27-1/1^{N}/1^{A} is detected in the presence of GST-SCAR2-LIP1 using an anti-MBP antibody; the bottom panel shows the total protein stained by Coomassie brilliant blue. MBP protein and GST protein were used as negative controls. Arrows indicate specific bands of purified proteins.

Other supporting materials for this manuscript include the following:

Video S1. SBEM 3D reconstruction of a dividing cell.

Video S2. Cell plate expansion in Col-0.

Video S3. Cell plate expansion in the *vap27-1346* mutant.

912 **Supplemental Tables**

913 **Table S1. Candidate proteins obtained from the SCAR2 Y2H screen**

Accession	Information
at1g21280	Expressed protein
at2g12440	Expressed protein
at3g30300	Similar to vesicle-associated membrane
at4g02060	MCM7, PRL (PROLIFERA); ATP binding / DNA binding / DNA-dependent atpase
at2g24270	NADP-dependent glyceraldehyde-3-phosphatase dehydrogenase
at2g25760	Protein kinaze REVERSE
at5g37445	Pseudogene
at4g13830	DNAJ heat shock N-terminal domain containing protein (J20)
at2g39770	GDP-mannose pyrophosphorylase
at1g77720	Protein kinase family protein
at3g60600	Symbols: VAP, (AT)VAP, VAP27, VAP27-1
at3g23580	Rnr2, rnr2a (ribonucleotide)
at5g39410	Identical to Probable mitochondrial saccharopine dehydrogenase
at3g17350	Similar to unknown protein
at1g21880	LYM1 / peptidoglycan-binding lysm domain containing protein
at3g16640	Tctp (translationally controlled tumor protein

914

915 **Table S2. The list of plasmids constructed in this research.**

DNA fragment	Destination vector	Fusion protein
pVAP27-1:VAP27-1	pMDC107	pVAP27-1:VAP27-1-mCherry
SCAR2 full-length	pMDC43-nYFP	nYFP-SCAR2
SCAR2 $^{\Delta LIP1}$		nYFP-SCAR2 $^{\Delta LIP1}$
SCAR2 $^{\Delta LIP2}$		nYFP-SCAR2 $^{\Delta LIP2}$
SCAR2 $^{\Delta LIP3}$		nYFP-SCAR2 $^{\Delta LIP3}$
VAP27-1 full-length CDS	pMDC43-cYFP	cYFP-VAP27-1
VAP27-1^{N}		cYFP-VAP27-1^{N}
VAP27-1^{A}		cYFP-VAP27-1^{A}
SCAR1 full-length CDS	pGADT7	AD-SCAR1
SCAR2 full-length CDS		AD-SCAR2
SCAR3 full-length CDS		AD-SCAR3
SCAR4 full-length CDS		AD-SCAR4
SCAR2 (a.a.1-432)		AD-SCAR2 (a.a.1-432)
SCAR2 (a.a.357-967)		AD-SCAR2 (a.a.357-967)
SCAR2 (a.a.800-1399)		AD-SCAR2 (a.a.800-1399)
SCAR2 (a.a.1-109)		AD-SCAR2 (a.a.1-109)
SCAR2 (a.a.100-236)		AD-SCAR2 (a.a.100-236)
SCAR2 (a.a.229-346)		AD-SCAR2 (a.a.229-346)
SCAR2 (a.a.340-432)		AD-SCAR2 (a.a.340-432)
SCAR2 $^{\Delta LIP1}$		AD-SCAR2 $^{\Delta LIP1}$
SCAR2 $^{\Delta LIP2}$		AD-SCAR2 $^{\Delta LIP2}$
SCAR2 $^{\Delta LIP3}$		AD-SCAR2 $^{\Delta LIP3}$
VAP27-1$^{\Delta TMD}$	pGBKT7	BD-VAP27-1
VAP27-3$^{\Delta TMD}$		BD-VAP27-3

VAP27-4$^{\Delta TMD}$		BD-VAP27-4
VAP27-5 full-length CDS		BD-VAP27-5
VAP27-6$^{\Delta TMD}$		BD-VAP27-6
VAP27-9 full-length CDS		BD-VAP27-9
VAP27-10 full-length CDS		BD-VAP27-10
VAP27-1^{N}		BD-VAP27-1^{N}
VAP27-1^{A}		BD-VAP27-1^{A}
SCAR2 (a.a.1-432)	pGEX-4T1	GST-SCAR2 (a.a.1-432)
VAP27-1 full-length CDS	pMAL-c5X	MBP-VAP27-1
pVAP27-1:VAP27-1		pVAP27-1:VAP27-1-HA
pVAP27-1:VAP27-1^{N}	pROE-O4	pVAP27-1:VAP27-1^{N}-HA
pVAP27-1:VAP27-1^{A}		pVAP27-1:VAP27-1^{A}-HA
pSCAR2:SCAR2	Modified pMDC43	pSCAR2:SCAR2-HA
pSCAR2:SCAR2$^{\Delta LIP1}$		pSCAR2:SCAR2$^{\Delta LIP1}$-HA

Table S3. The primers used in this study.

Primer name	Sequence
AD-SCAR1-all-F	CCATGGAGGCCAGTGAATTCATGCCGCTTGTTAGGCTCCA
AD-SCAR1-all-R	AGCTCGAGCTCGATGGATCCTGTGTCGCTATCGCTCCATG
AD-SCAR3-all-F	CCATGGAGGCCAGTGAATTCATGCCACGGAATGTATACGG
AD-SCAR3-all-R	AGCTCGAGCTCGATGGATCCCGTATCACTCCATGTATCGC
AD-SCAR4-all-F	CCATGGAGGCCAGTGAATTCATGGCATTGACGAGATACCA
AD-SCAR4-all-R	AGCTCGAGCTCGATGGATCCCTCGCTCCAGCTATCTGAAT
AD-SCAR2-all-F	CCATGGAGGCCAGTGAATTCATGCCGTTGACGAGGTAC
AD-SCAR2-all-R	AGCTCGAGCTCGATGGATCCAGAATCACTCCAACTATCTG
AD-SCAR2-R-1	AGCTCGAGCTCGATGGATCCAAAATGAAAACTGAGGTGG
AD-SCAR2-F-2	CCATGGAGGCCAGTGAATTCATGGGTCCGTGGAACAACTATT
AD-SCAR2-R-2	AGCTCGAGCTCGATGGATCCAGAACCCTTCCCACGA
AD-SCAR2-F-3	CCATGGAGGCCAGTGAATTCATGGCGGGAGATGCTTCACCTACT
AD-SCAR2-1-P1-F	CCATGGAGGCCAGTGAATTCATGCCGTTGACGAGGTAC
AD-SCAR2-1-P1-R	AGCTCGAGCTCGATGGATCCTTCCACACCTTTGTTAGAGAA
AD-SCAR2-1-P2-F	CCATGGAGGCCAGTGAATTCATGGGTGTGGAATGGCATCCG

AD-SCAR2-1-P2-R	AGCTCGAGCTCGATGGATCCTTTCAACTTCACAACGCGCGC
AD-SCAR2-1-P3-F	CCATGGAGGCCAGTGAATTCATGGCGCGCGTTGTGAAGTTG
AD-SCAR2-1-P3-R	AGCTCGAGCTCGATGGATCCCTCATTGTATGTAGATTCAGG
AD-SCAR2-1-P4-F	CCATGGAGGCCAGTGAATTCATGGAATCTACATACAATGAG
AD-SCAR2-1-P4-R	AGCTCGAGCTCGATGGATCCAAATGAAAACTGAGGTGGGTC
BD-VAP27-1-F	CATGGAGGCCGAATTCATGAGTAACATCGATCTGATT
BD-VAP27-1-R	TGCGGCCGCTGCAGGTCGACTGTCCTCTTTTGGCTCTTTTTGCTTTC
BD-VAP27-3-F	CATGGAGGCCGAATTCATGAGTAACGAGCTTCTC
BD-VAP27-3-R	TGCGGCCGCTGCAGGTCGACTGTCCTCTTCTTACTTCT
BD-VAP27-4-F	CATGGAGGCCGAATTCATGACCGGCGTTGGCGAGAAT
BD-VAP27-4-R	TGCGGCCGCTGCAGGTCGACTGTGGGAGAAGCTAAGGTAAGTTTGCTGTTCCTCTGGTT
BD-VAP27-5-F	CATGGAGGCCGAATTCATGAAGAATGTGAATCGAGTC
BD-VAP27-5-R	TGCGGCCGCTGCAGGTCGACATGTTGCTTTCGTCTTCTTGA
BD-VAP27-6-F	CATGGAGGCCGAATTCATGACGACCGGAGATCTCGTT
BD-VAP27-6-R	TGCGGCCGCTGCAGGTCGACTATCCGGTTCTGCTTCTTGCTTGTTTCTTT
BD-VAP27-8-F	CATGGAGGCCGAATTCATGACTATGACGGAGGAGAAA
BD-VAP27-8-R	TGCGGCCGCTGCAGGTCGACGACAGAGTCAGCTCCTTCGCC

BD-VAP27-9-F	CATGGAGGCCGAATTCATGGCTTTAACGGAGGACAAA
BD-VAP27-9-R	TGCGGCCGCTGCAGGTCGACAGCAGCGTCTACTCCTCCTTG
BD-VAP27-10-F	CATGGAGGCCGAATTCATGCCAATAGGTGACCGTCAG
BD-VAP27-10-R	TGCGGCCGCTGCAGGTCGACGGACAAAGAATCTACGGATTC
attB-SCAR2-CDS-F	GGGGACAAGTTTGTACAAAAAAGCAGGCTGCATGCCGTTGACGAGGTAC
attB-SCAR2-CDS-R	GGGGACCACTTTGTACAAGAAAGCTGGGTGAGAATCACTCCAACTATCTG
proSCAR2-HindIII-F	ACGACGGCCAGTGCCAAGCTTTAGCGGTGAGCGTTAGTC
proSCAR2-KnpI-R	ACTCATTTTTTCTACCGGTACCAGTGACCGACCACCATTA
SCAR2-KpnI-HA-F	AGACAGAGAAGCTCAAACAGGTACCATGCCGTTGACGAGGTACCAAT
SCAR2-SpeI-HA-R	TCTAGAACTAGTTCAGGCGTAGTCGGGCACGTCGTAGGGGTAAGAATCACTCCAACTAT
pENTR-SCAR2$^{\Delta LIP1}$-F	AGGATTCACAAATGGAGTCGGAAACAGAAACAGACGATGAGTGT
pENTR-SCAR2$^{\Delta LIP1}$-R	GTTTCCGACTCCATTTGTGAATCCTGTGTAATAGTTGTTCCA
pENTR-SCAR2$^{\Delta LIP2}$-F	ATCAGATACTTTGATGGAGGACCCACCTCAGTTTTCATTTTC
pENTR-SCAR2$^{\Delta LIP2}$-R	GTGGGTCCTCCATCAAAGTATCTGATCTACTCTTAGGTCTAC
pENTR-SCAR2$^{\Delta LIP}$3-F	TTGAAGAGAGAATGGAGGACTTTTCTCATTCAAATGGAAACA
pENTR-SCAR2$^{\Delta LIP3}$-R	TTTGAATGAGAAAAGTCCTCCATTCTCTCTTCAACCGCATCA

pROE-O4-proVAP27-1-F	GGGCGCCCCGCGGAAAGCTTTTCATATCGGCTTCTTACTCTTTAAT
pROE-O4-proVAP27-1-R	CAAGGCCTTCTAGAAAAACTCGAGCCCGATCAGATCGCC
pROE-O4-VAP27-1-KpnI-F	ACCCGGGAGAATTCGTCGACATGAGTAACATCGATCTGATTGGGATGAGTAACC
pROE-O4-VAP27-1-SalI-R2	GGGATATCACTAGTAAAAGGTACCTTAAGCGTAATCTGGAACATCGTATGG
pROE-O4-VAP27-1-HA-R1	AGCGTAATCTGGAACATCGTATGGGTATGTCCTCTTCATAATGTATCCCAAA
GST-SCAR2-F	TCGGATCTGGTTCCGCGTGGATCCATGCCGTTGACGAGGTAC
GST-SCAR2-R	TCAGTCACGATGCGGCCGCTCGAGAAAATGAAAACTGAGGTGG
MBP-VAP27-1-F	TCGAGGGAAGGATTTCACATATGATGAGTAACATCGATCTGATTG
MBP-VAP27-1-R	TTACCTGCAGGGAATTCGGATCCTGTCCTCTTCATAATGTAT